AD-A062 660 ENVIRONMENTAL RESEARCH INST OF MICHIGAN ANN ARBOR F/G 20/6
THERMOPLASTIC MODULATOR DEVELOPMENT.(U)
JUN 78 W S COLBURN, C C ALEKSOFF, I CINDRICH F33615-77-C-1019
UNCLASSIFIED ERIM-128700-10-F AFAL-TR-78-86 NL

1 OF 1
ADA
062660

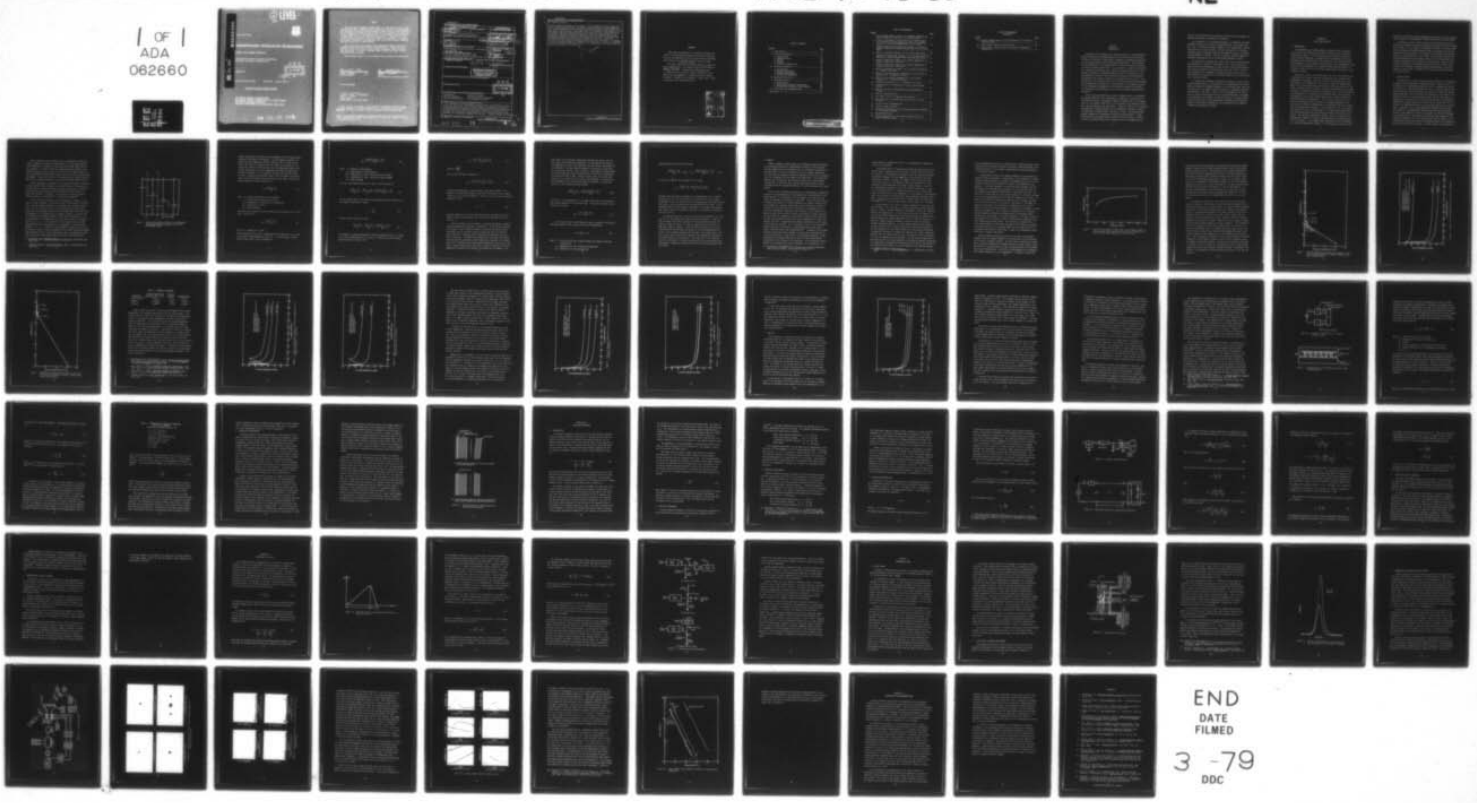

END
DATE
FILMED
3 -79
DDC

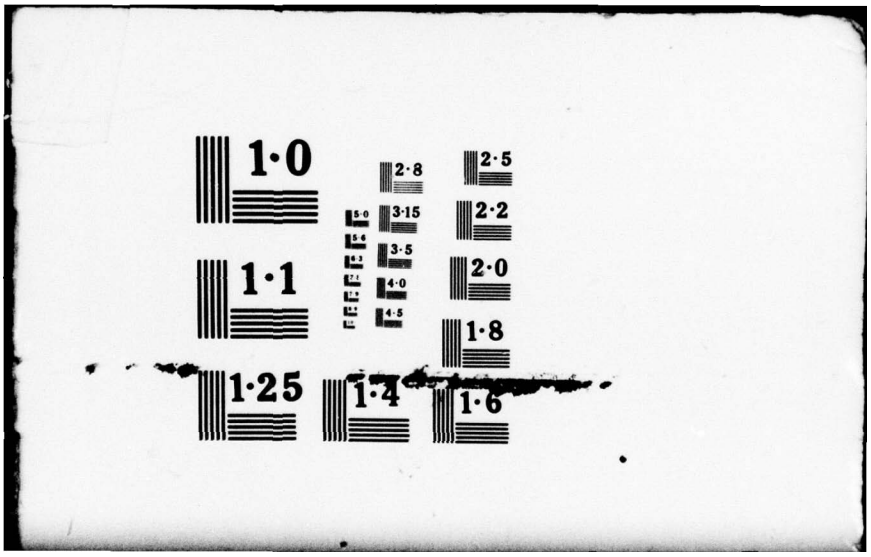
1·0
1·1
1·25
1·4
1·6
1·8
2·0
2·2
2·5
2·8
3·15
3·5
4·0
4·5

(2) LEVEL II

NW

AFAL-TR-78-86

THERMOPLASTIC MODULATOR DEVELOPMENT

Radar and Optics Division

Environmental Research Institute of Michigan
Box 8618, Ann Arbor, Michigan 48107

JUNE 1978

Final Technical Report April 1977 - January 1978

AIR FORCE AVIONICS LABORATORY
AIR FORCE WRIGHT AERONAUTICAL LABORATORIES
AIR FORCE SYSTEMS COMMAND
WRIGHT-PATTERSON AIR FORCE BASE, OHIO 45433

NOTICE

When Government drawings, specifications, or other data are used for any purpose other than in connection with a definitely related Government procurement operation, the United States Government thereby incurs no responsibility nor any obligation whatsoever; and the fact that the Government may have formulated, furnished, or in any way supplied the said drawings, specifications, or other data, is not to be regarded by implication or otherwise as in any manner licensing the holder or any other person or corporation, or conveying any rights or permission to manufacture, use, or sell any patented invention that may in any way be related thereto.

This final report was submitted by Environmental Research Institute of Michigan, Ann Arbor, Michigan 48107, under Contract No. F33615-77-C-1019, Project No. 2001, with the Air Force Avionics Laboratory, Wright-Patterson AFB, Ohio 45433. Dr. David L. Flannery, DHO-2, was the Air Force Avionics Laboratory Project Engineer.

This technical report has been reviewed and is approved for publication.

David L. Flannery
DAVID L. FLANNERY
Project Engineer

Kenneth R. Hutchinson
KENNETH R. HUTCHINSON
Chief
E-O Techniques and Applications Grp

FOR THE COMMANDER

Ronald F. Paulson
RONALD F. PAULSON
Acting Chief
Electro-Optics Technology Branch

"If your address has changed, if you wish to be removed from our mailing list, or if the addressee is no longer employed by your organization please notify AFAL/DHO *, W-PAFB, OH 45433 to help us maintain a current mailing list".*

Copies of this report should not be returned unless return is required by security considerations, contractual obligations, or notice on a specific document.

UNCLASSIFIED

SECURITY CLASSIFICATION OF THIS PAGE *(When Data Entered)*

REPORT DOCUMENTATION PAGE

READ INSTRUCTIONS BEFORE COMPLETING FORM

1. REPORT NUMBER: AFAL-TR-78-86	2. GOVT ACCESSION NO.
3. RECIPIENT'S CATALOG NUMBER	
4. TITLE *(and Subtitle)*: THERMOPLASTIC MODULATOR DEVELOPMENT.	5. TYPE OF REPORT & PERIOD COVERED: Final Technical Report. 11 Apr 77 - Jan 78,
6. PERFORMING ORG. REPORT NUMBER: ERIM-128700-10-F	
7. AUTHOR(s): W.S. Colburn, C.C. Aleksoff, I. Cindrich	8. CONTRACT OR GRANT NUMBER(s): F33615-77-C-1019
9. PERFORMING ORGANIZATION NAME AND ADDRESS: Environmental Research Institute of Michigan, P.O. Box 8618, Ann Arbor, MI 48197	10. PROGRAM ELEMENT, PROJECT, TASK AREA & WORK UNIT NUMBERS: 2001-02-46 02
11. CONTROLLING OFFICE NAME AND ADDRESS: Air Force Avionics Laboratory (DHO), Air Force Wright Aeronautical Laboratories, Wright-Patterson AFB, Ohio 45433	12. REPORT DATE: June 1978 13. NUMBER OF PAGES: vii + 71
14. MONITORING AGENCY NAME AND ADDRESS *(if different from Controlling Office)*	15. SECURITY CLASS. *(of this report)*: Unclassified 15a. DECLASSIFICATION/ DOWNGRADING SCHEDULE

16. DISTRIBUTION STATEMENT *(of this Report)*

DISTRIBUTION STATEMENT A
Approved for public release; Distribution Unlimited

62204F

17. DISTRIBUTION STATEMENT *(of the abstract entered in Block 20, if different from Report)*

DDC RECEIVED DEC 29 1978 B

18. SUPPLEMENTARY NOTES

19. KEY WORDS *(Continue on reverse side if necessary and identify by block number)*

Thermoplastic	Optical Processing
Real-Time Modulator	Real-Time Optical Processing
Spatial Light Modulator	Electron-Beam Recording

20. ABSTRACT *(Continue on reverse side if necessary and identify by block number)*

An analytical and experimental research effort was performed to investigate the application of an existing breadboard thermoplastic modulator to wideband spectrum analysis by means of real-time optical data processing. The objectives of the research were identification of an approach for increasing the cycling rate of the modulator to 10 frames per second and improvement of the modulator bandwidth to 100 MHz. A computer model was estab-

DD FORM 1 JAN 73 1473 EDITION OF 1 NOV 65 IS OBSOLETE

UNCLASSIFIED

SECURITY CLASSIFICATION OF THIS PAGE *(When Data Entered)*

407 903

78 12 26 063

20. Abstract continued

lished to predict the transient thermal behavior of the thermoplastic substrate under conditions of continuous rapid cycling. The computer analysis revealed that the key parameters are the thermal conductivity of the substrate, the substrate thickness, and the length of the heat pulses. Based on results of the computer model, the recommended design employs a 6 mm thick sapphire substrate that is heated with 1 msec pulses and that is liquid cooled on the rear surface. The system bandwidth was analyzed in terms of the impulse responses of the subsystems, including the electron beam modulation, the electron beam spot size, and the thermoplastic response. An analysis of the recording duty cycle led to recommended changes to the deflection circuits to increase the recording duty cycle, with a goal of 97%. Modifications to the breadboard thermoplastic modulator included installation of a new input to reduce the impedance mismatch and redesign of the cathode support structure to accommodate new cathodes. Although limited by a 25 μm spot size, thermoplastic recordings were achieved at input frequencies of up to 120 MHz.

micron

FOREWORD

This report was prepared by the Radar and Optics Division of the Environmental Research Institute of Michigan. The work was sponsored by the Air Force Avionics Laboratory under Contract No. F33615-77-C-1019, Project No. 2001.

The report covers work performed between 11 April 1977 and 11 January 1978. The contract monitor is Dr. David L. Flannery, AFAL/DHO. The principal investigators are I. Cindrich and W.S. Colburn. Major contributors to the report are C.C. Aleksoff, I. Cindrich, and W.S. Colburn. B. Betke, M. Gredell, C.D. Leonard, G. Orbits, and C. Stout contributed to the technical effort.

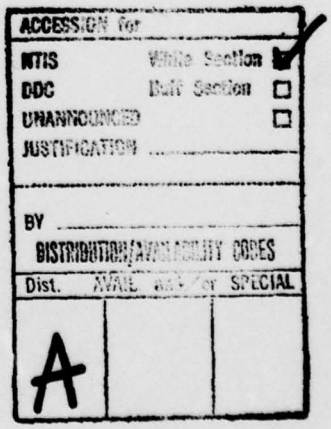

TABLE OF CONTENTS

LIST OF ILLUSTRATIONS

LIST OF ILLUSTRATIONS
(Continued)

SECTION I
INTRODUCTION

During the last several years, research efforts at the Environmental Research Institute of Michigan supported by the Air Force Avionics Laboratory have succeeded in developing a breadboard thermoplastic modulator for real-time coherent optical processing applications. These research efforts culminated in the demonstration of real-time optical processing of synthetic aperture radar data. In this report, we present the results of a research investigation that considered the application of the thermoplastic modulator to wideband spectrum analysis. Constraints on the thermoplastic cycling rate have previously limited the effectiveness of the modulator for spectrum analysis by requiring a low duty cycle. The objectives of this research effort were to identify one or more techniques for increasing the cycling rate of the modulator to 10 frames per second. We also developed improvements in the modulator bandwidth and methods for increasing the recording duty cycle of the electron beam deflection subsystem.

In the cycle time analysis, we used a computer model to investigate the thermal behavior of the thermoplastic faceplate at cycling rates of 10 frames per second. The computer analysis revealed that the key parameters are the thermal conductivity of the substrate, the substrate thickness, and the length of the heat pulses. Using the results of the analysis, we established a design approach for a thermoplastic faceplate in which the substrate is sapphire with a thickness of 6 mm. The average thermoplastic temperature is minimized by applying heating pulses of 1 msec duration and by providing liquid cooling at the rear surface. Cooling at the rear surface leads to the requirement that the thermoplastic be

read out in reflection and thus imposes the additional requirement that unwanted reflections be minimized or separated.

In an analysis of the recording bandwidth, we expressed the system bandwidth in terms of the electron beam modulation, the electon beam spot size, the spatial frequency response of the thermoplastic, and the sweep speed of the electron beam. We used the analysis to establish component impulse response parameters that together lead to an overall system bandwidth of 100 MHz. We also developed a detailed analysis to determine the bandwidth of the electron beam modulation circuit.

We analyzed the recording duty cycle, which on the existing breadboard modulator is limited to about 50% or less. The result of our analysis was the establishment of three retrace circuit configurations that should be capable of increasing the duty cycle to 97%. Of the three approaches, we recommend a resonant recovery retrace circuit in which energy is transferred from a resonant capacitor to the deflection coil to provide retrace.

In testing the breadboard thermoplastic modulator we made two important modifications, the installation of a feedthrough for the video signal to reduce the impedance mismatch to the coaxial signal feed, and the redesign of the cathode support structure to accommodate cathodes obtained from a new vendor. With the new feedthrough we were able to observe electron beam modulation and to form thermoplastic recordings at frequencies up to 120 MHz. We observed that at a constant thermal bias, the decay time of the thermoplastic recording was strongly dependent on the spatial frequency of the recording, with the highest frequencies decaying most rapidly.

SECTION II

CYCLE TIME ANALYSIS

1. INTRODUCTION

The thermoplastic recording medium is generally used in applications that do not require rapid cycling, by which we mean repetitive writing and erasing. In the spectrum analysis application, however, rapid cycling is important to minimize data lost between write cycles. Consequently an important part of the research effort reported herein was an analysis of the thermal characteristics of the thermoplastic faceplate, and the development of a faceplate design approach capable of achieving a cycle rate of 10 Hz without significantly reducing the thermoplastic lifetime.

During the course of one write/erase cycle, heat is necessary both to develop and to erase the surface deformations that constitute the thermoplastic recording. There are two modes of heating, which can be used singly or in combination. One mode of cycling the thermoplastic makes use of rapid heating during the develop and erase portions of the cycle, followed by rapid cooling to freeze the thermoplastic, and slower cooling of the substrate to remove accumulated heat. In the second mode, the thermoplastic is maintained in a thermally biased state such that deformations form and erase spontaneously after a charge distribution is written onto the thermoplastic. In the latter case, the rates at which the deformations form and decay are strongly dependent on the temperature at which the thermoplastic is maintained, the rates increasing as the temperature increases. For operation at 10 Hz it is presumably possible to bias the thermoplastic at a sufficiently high temperature that deformations occur and decay well within the 100 msec cycle period. The necessary temperature, however, must be so high that the thermoplastic behaves as a liquid, acquiring most of the limitations of an oil film device. The constant high temperature may also contribute to a reduced thermoplastic lifetime. Our investigation, therefore, was

directed at developing a design employing pulsed heating in which significant cooling of the thermoplastic takes place between each heat pulse.

The method we used to study the cycle time characteristics was to model with a computer program one-dimensional transient heat flow through the substrate. In our analysis we examined the effect of various parameters, including the substrate material and its thickness, the rate of cooling at the rear surface of the substrate, the length of the heating pulse, and the temperature of the coolant. We found that the most important parameters were the thermal conductivity of the substrate, the substrate thickness, and the length of the heat pulse. Based on the results obtained with our computer model and certain practical considerations, we developed a faceplate design incorporating a 6 mm thick sapphire substrate that is heated with 1 msec pulses and liquid cooled on the rear surface.

2. SUBSTRATE MODEL

The dynamics of the heat flow through the substrate were determined by means of a one-dimensional transient analysis. Since we were concerned with the instantaneous temperature at the thermoplastic surface in response to a repetitive pulsed heat input, a transient analysis was clearly required. Upon consideration of the rate of heat flow through physical materials and of the amount and frequency of heat input to the substrate surface, it quickly became evident that the only practical approach was to remove the heat from the rear surface of the substrate; schemes that assumed radial flow of heat from the active area of the substrate to regions beyond the active area were therefore not investigated. Although a two or three dimensional analysis would have been more complete, a one-dimensional analysis was nevertheless adequate because of the symmetry provided by the geometry in which the diameter of the heated area on the substrate surface was large compared to the substrate thickness, and in the limiting case near the center of the active area, the heat flow could be considered normal to the heated surface in the direction of the rear, or cooled surface of the substrate.

Heat is gained or lost through one or a combination of three processes: conduction, convection, and radiation. At the heated surface of the substrate, we assumed all heat loss was through conduction into the substrate. No heat is given up through convection because of the vacuum envelope, and heat losses due to radiation are small because of the low temperature differential between the surface and the surrounding environment. At the rear surface of the substrate, we assumed that heat was given up through convection, in particular through liquid cooling.

Several approaches are possible for solving the transient conduction of heat through a slab of material of infinite extent. The method described here is a numerical approach in which the material is divided into many thin slabs, and the heat flow between the thin slabs in a small time interval is computed. In particular, we used the General Numerical Method of Dusinberre[1] as presented by McAdams[2].

If we consider the substrate to be divided into a number of thin slabs of equal thickness, we can write a heat balance equation for each slab. The heat balance equation is a statement that the heat flowing into or out of a slab is equal to the net change in the heat stored within the slab (assuming no sources of heat generation within the slab). The geometry we are concerned with is shown in Figure 1; the substrate is divided into an integral number of slabs each of thickness Δx. We are interested in the temperature T_0 at the front surface, the temperatures T_1, T_2, T_3, ... at the center of each successive slab, and the temperature T_n at the rear surface of the substrate. The solid lines labelled 1, 2, 3, ... in Figure 1 pass through the center of each slab; the volume of slab 1 is thus represented by the region between the dashed lines labelled A and B. We are interested, then, in computing the heat flow across each of the dashed lines and the heat stored within the

1. Dusinberre, G.M., Numerical Analysis of Heat Flow, McGraw-Hill, New York, 1949.

2. McAdams, William H., Heat Transmission, Chapt. 2, McGraw-Hill, New York, 1954.

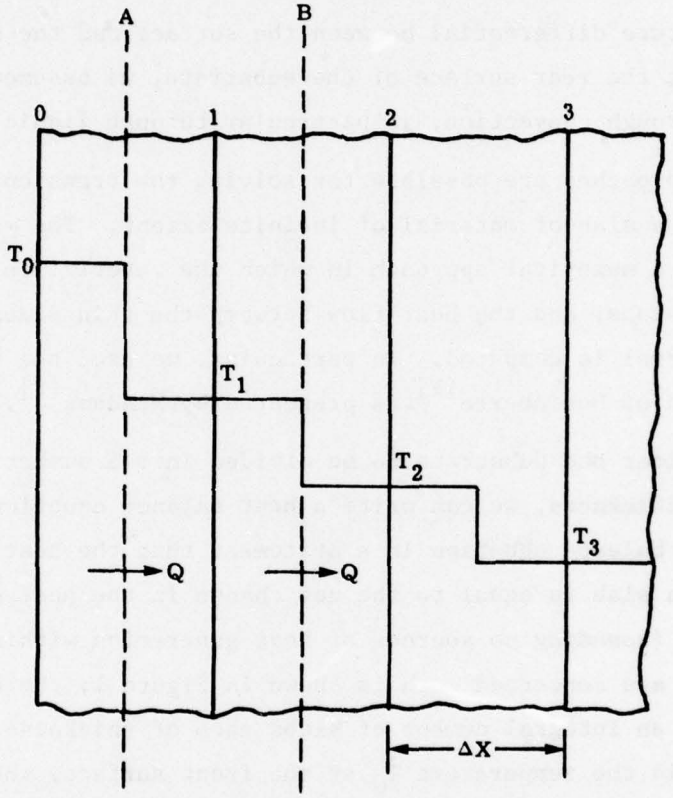

Figure 1. Cross Section Sketch of Part of the Substrate Showing the Slab Configuration Assumed for the Computer Model

volume between them (we assume a third dimension of unit length perpendicular to the plane of the figure). In this numerical approach, we assume that the temperature varies stepwise from the center of one slab to the center of adjacent slabs (as shown in the figure); if we choose the slabs to be sufficiently thin, the temperature profile will closely approximate the actual temperature variation throughout the substrate thickness. Let us consider the heat flow into the volume of slab 1, between the two dashed lines A and B in Figure 1; the heat flow in one time increment from the surface 0 into slab 1 (across the dashed boundary A) can be expressed as

$$\Delta Q = \frac{kA(T_0 - T_1)}{\Delta x} \tag{1}$$

where k = thermal conductivity of the material
A = cross section surface area of slab
T_0 = temperature of the surface of the material
T_1 = temperature of slab 1
Δx = slab thickness.

Similarly we can express the heat flowing across the dashed line B from slab 1 to slab 2 as

$$\Delta Q = \frac{kA(T_1 - T_2)}{\Delta x} \tag{2}$$

where T_2 = temperature of slab 2.

Note that since the ΔQ in Eq. 2 represents heat flowing out of the slab, it will have a sign opposite to ΔQ in Eq. 1. The net change in heat stored within slab 1 can be expressed as

$$\Delta Q = \frac{(A\Delta x)(\rho c_p)(T_1' - T_1)}{\Delta t} \qquad (3)$$

where ρ = density of the material

c_p = heat capacity of the material

T_1' = temperature of slab 1 after the time increment

T_1 = temperature of slab 1 before the time increment

Δt = time increment.

The total heat balance equation for slab 1 can be written as

$$\frac{kA(T_0 - T_1)}{\Delta x} - \frac{kA(T_1 - T_2)}{\Delta x} = \frac{(A\Delta x)(\rho c_p)(T_1' - T_1)}{\Delta t} \qquad (4)$$

We can combine some of the variables by making use of the definition of the thermal diffusivity α, where

$$\alpha = \frac{k}{\rho c_p} \qquad (5)$$

The heat balance equation is then

$$\frac{A(T_0 - T_1)}{\Delta x} - \frac{A(T_1 - T_2)}{\Delta x} = \frac{(A\Delta x)(T_1' - T_1)}{\alpha \Delta t} \qquad (6)$$

The equation is usually rearranged to give an expression for T_1' in terms of the other temperatures, T_0, T_1, and T_2. Thus we can write the heat balance equation for slab 1 as

$$T_1' = \frac{T_0 + (M - 2)T_1 + T_2}{M} \tag{7}$$

where $M = \frac{(\Delta x)^2}{\alpha \Delta t}$,

and for the i^{th} slab the equation is

$$T_i' = \frac{T_{i-1} + (M - 2)T_i + T_{i+1}}{M} \tag{8}$$

To prevent instabilities in the solutions, the time increment Δt is chosen to be sufficiently small so that the coefficients of the temperatures T_0, T_1, T_2 are never negative. From Eq. 8 we see that the stability condition is that

$$M - 2 \geq 0 \tag{9}$$

From the definition of M it is seen that a small slab dimension Δx may require a small time increment Δt to satisfy the stability criterion of Eq. 9.

The free surfaces of the material are treated separately, considering the mechanism for heat loss or absorption. At the surface labelled 0 in Figure 1, heat is added by means of resistive heating during the heat pulse, and it is given up only by conduction into the substrate since there is no convection and we assumed negligible heat transfer due to radiation. To simplify the computation, we assumed that during the heat pulse the substrate surface temperature increased at a uniform rate until it reached a specified maximum temperature at the end of the pulse. Given a fixed rate of heat input (resistive heating), the actual temperature increase is not uniform, but depends on the length of the

heat pulse, the temperature differential between the surface and the next slab, and the material properties. We also ignored the effect of the thermoplastic layer, and considered only the surface temperature of the substrate. The heat balance equation is now applied to the slab at the substrate surface, which in Figure 1 comprises the volume between the surface labelled 0 and the dashed line A; note that the thickness of this surface slab is $\frac{1}{2}\Delta x$. During the heat pulse, the surface temperature T_0' at the end of the current time increment is a function of the assumptions about how the heat input is simulated. Between heat pulses, the heat balance equation becomes

$$-\frac{kA(T_0 - T_1)}{\Delta x} = \frac{(A\Delta x)(\rho c_p)(T_0' - T_0)}{2\Delta t} \qquad (10)$$

where the 2 in the denominator of the right hand side occurs because of the reduced thickness of the surface slab. Putting the equation in the form of Eq. 8 gives

$$T_0' = \frac{(M - 2)T_0 - 2T_1}{M} \qquad (11)$$

At the rear surface of the substrate, heat is removed by convection. The heat transfer to the cooling fluid can be expressed as

$$\Delta Q = hA(T_n - T_f) \qquad (12)$$

where h = coefficient of heat transfer between the substrate and the cooling fluid

T_n = temperature of rear surface of the substrate

T_f = temperature of the cooling fluid.

The heat balance equation then becomes

$$\frac{kA(T_{n-1} - T_n)}{\Delta x} - hA(T_n - T_f) = \frac{(A\Delta x)(\rho c_p)(T_n' - T_n)}{2\Delta t} \qquad (13)$$

If we let $N = \frac{h\Delta x}{k}$ we can rearrange Eq. 13 to give

$$T_n' = \frac{2NT_f - [M - (2N + 2)]T_n + 2T_{n-1}}{M} \qquad (14)$$

Although this heat balance equation is straightforward and is readily solved to give T_n', the coefficient of heat transfer h is not easily determined, as it is a function of the cooling geometry, the fluid flow over the surface, and the properties of the substrate and the fluid. A considerable amount of heat transfer literature is concerned with predicting h under various circumstances, and most of the methods are based on empirical results.

Our approach then was to solve the heat balance equations (7), (11), and (14) for the temperatures after each time increment Δt. Since the time increments were small compared to the cycle period and since the number of slabs was large, we solved the equations with the aid of a high speed digital computer. Given the computer program as a tool for simulating heat flow through the substrate, we then investigated the effect of the substrate material and thickness, the cooling rate at the rear surface, and the heat pulse length, on the temperature variation of the heated surface of the substrate. The objective of our investigation was to determine a faceplate configuration that would maintain the thermoplastic temperature significantly below the peak temperature used for erasure.

3. RESULTS

Using a computer program based on the numerical approach described in the previous section, we investigated the effect on the substrate surface temperature of the material type, its thickness, the length of the heat pulse, the rate of convection, and the coolant temperature. We found that the parameters having the greatest effect are the material type, its thickness, and the length of the heat pulse. From the investigation, we conclude that the substrate should have a high thermal conductivity, it should be thin, and the heat pulse should be short; an example would be a sapphire substrate 6.3 mm thick heated with 1 msec pulses.

Since we are ultimately interested in the thermoplastic temperature, in most of our investigations we determined the time dependence of the heated surface of the substrate over the length of one cycle (in all cases, we assumed a cycle period of 100 msec). As our interest here is to compare the effects of various parameters, we assume a simple cycle that consists of a single, initial heat pulse followed by a period of cooling until the next heat pulse initiates the succeeding cycle; a practical thermoplastic modulator would probably use two separate heat pulses in each cycle to better control the develop and erase functions. For the purpose of comparison, we arbitrarily assume in each case that the heat pulse raises the substrate surface temperature to a peak temperature of 120°C, a temperature that might reasonably be used to erase a thermoplastic recording. Such a temperature was, in fact, measured during a 540 msec erase pulse of a photoplastic device that used a highly stabilized ester resin thermoplastic[3]. Although a still higher temperature would have been required to erase surface deformations in the ester resin with a 1 msec pulse, the softening temperature of that thermoplastic was higher than that of the octyl decal methacrylate thermoplastic we are using for the modulator. In the absence of experimental data concerning the actual response of the thermoplastic to

3. Colburn, W.S. and DuBow, J.B., "Photoplastic Recording Materials," Final Technical Report, AFAL-TR-73-255, August 1973.

1 msec pulses, we believe that 120°C is a reasonable peak temperature to use in our analysis.

As mentioned above, we assumed that during the heat pulse the substrate surface temperature rises uniformly to reach 120°C at the end of the pulse. The temperature increase is thus the difference between the initial temperature at the beginning of the pulse and the final temperature of 120°C. Cooling, we assumed, is by forced convection at the rear surface of the substrate, with the coefficient of heat transfer h in the range that would imply liquid cooling. In most of our simulations we assumed for the heat transfer coefficient a value of 1.0 cal/(sec)(cm^2)(°C). Although the choice for h is rather arbitrary, as with the peak erase temperature in the absence of experimental data it is difficult to proceed other than by making a reasonable estimate. The value we chose actually lies somewhat above the range given by McAdams[4] for water cooling without a phase change (i.e., boiling).

We used either of two sets of initial conditions to begin the computer solution. The first set of conditions assumed that the substrate was at a constant, uniform temperature throughout, usually 20°C (approximately room temperature). In this case, we were able to observe the rise in the average temperature of the heated surface (the computer program determined the average temperature for each 100 msec period), but needed to simulate several seconds of cycling in order to approach constant average parameters. To reach steady conditions more rapidly, we used the second set of initial conditions in which we specified an initial temperature of the heated surface, and the program established a temperature distribution through the substrate as a linear temperature gradient from the heated surface to the rear surface, which was assumed to be at the temperature of the coolant. For the initial temperature of the heated surface we usually specified the estimated ultimate average surface temperature, repeating the solution until the initial specified surface temperature was within one or two degrees of the computed average

4. McAdams, William H., Heat Transmission, p. 5, McGraw-Hill, New York, 1954.

surface temperature after ten or twenty cycles. Although several iterations were often required to obtain the proper initial conditions, the interactive nature of the computer program made for rapid convergence to the desired results.

In exercising the heat flow computer program, it was important to observe certain precautions. In particular, it was necessary to choose parameters that satisfied the stability requirement given by Eq. 9; the stability condition was verified by a check at the beginning of the program. It was also important to choose the time increment and the individual slab thickness small enough so that the discrete nature of the analysis would adequately approximate a continuous solution. In most of our simulations, we used a time increment of 0.25 msec, although in our early investigations we often used an increment of 2.5 msec. In much of our analysis we divided the substrate into 20 slabs, but used 40 to 60 in our final sets of solutions. The effect of the number of slabs on the accuracy of the solution is suggested by the curve in Figure 2, a plot of cooling achieved as a function of the number of slabs used in the simulation. The cooling is the difference of the heated surface temperature between its maximum (120°C) and minimum values, expressed as a percentage of the peak temperature. The data in Figure 2 were generated with a model in which the substrate was sapphire 9.5 mm thick heated with 10 msec pulses. From the curve it appears that a still larger number of slabs would have improved the solution accuracy, but we felt that 60 was an adequate number for the purpose of our investigation and given the uncertainty in some of the assumptions (such as the heat transfer coefficient).

Before presenting results in detail, we can make a few general comments about the thermal behavior of the substrate, and in particular of its first, or heated, surface. For most cases of interest, we found that the surface temperature decreased rapidly for about 10 msec following the end of the heat pulse, and then decreased slowly for the remainder of the cooling period. This effect is advantageous as it minimizes the average temperature of the thermoplastic. Secondly we found that

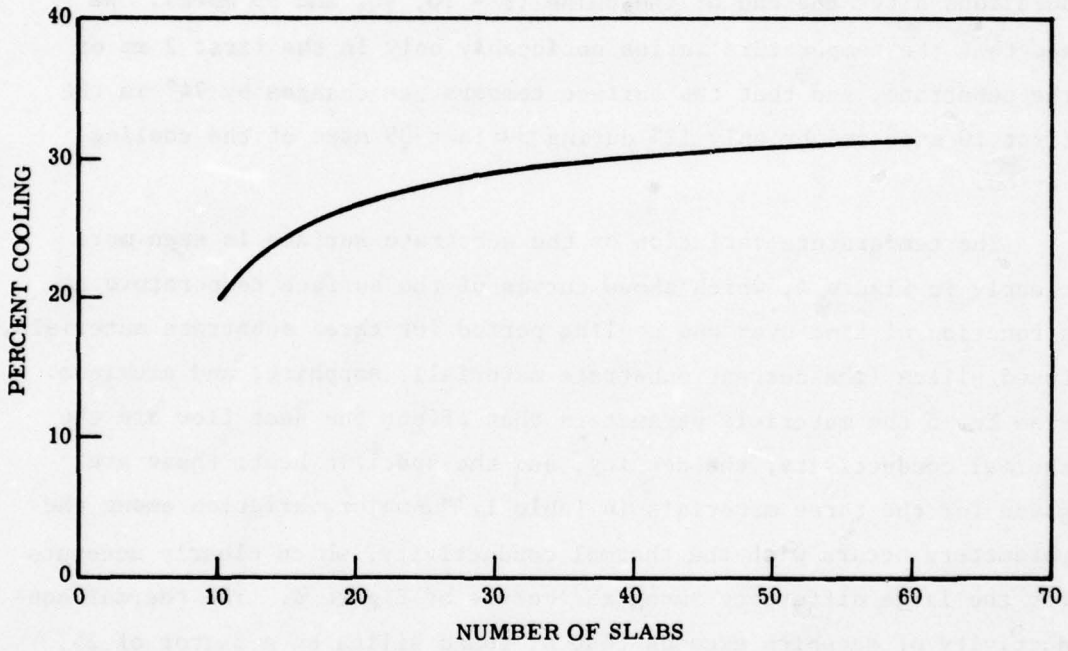

Figure 2. Effect of the Number of Slabs Used in the Computer Model on the Predicted Cooling During One Cycle for a Sapphire Substrate 9.5 mm Thick, Heated with 10 msec Pulses

at the end of the cooling period, the temperature distribution through substrate tended to be a linear decrease from the first to the second surface, with the latter a few degrees above the coolant temperature. This distribution was significantly affected by the heat pulse only in the layers relatively near the heated surface, and only for the first 10 or 20 msec following the heat pulse. Figure 3, for example, shows curves of the temperature distribution through a 6.3 mm thick sapphire substrate at the end of a 1 msec heat pulse (t = 0) and at several time durations after the end of the pulse (t = 10, 40, and 99 msec). We see that the temperature varies noticeably only in the first 2 mm of the substrate, and that the surface temperature changes by 74° in the first 10 msec and by only 12° during the last 89 msec of the cooling period.

The temperature variation of the substrate surface is seen more clearly in Figure 4, which shows curves of the surface temperature as a function of time over one cooling period for three substrate materials, fused silica (the current substrate material), sapphire, and aluminum. From Eq. 5 the materials parameters that affect the heat flow are the thermal conductivity, the density, and the specific heat; these are given for the three materials in Table 1. The major variation among the parameters occurs with the thermal conductivity, which clearly accounts for the large difference among the curves of Figure 4. The thermal conductivity of sapphire exceeds that of fused silica by a factor of 25, and the corresponding ratio for aluminum and fused silica is 148. Because of the low conductivity, the heat flow through the fused silica is slow compared to the assumed rate of heat removal at the rear surface. This conclusion is supported by the curves in Figure 5, which are comparable to those shown in Figure 3 with the only difference being the change in substrate material. Because of the relatively high rate of cooling at the rear surface of the substrate, there is only a small temperature drop at the substrate-coolant interface. Furthermore, the effect of the temperature variation extends only about 0.4 mm into the material.

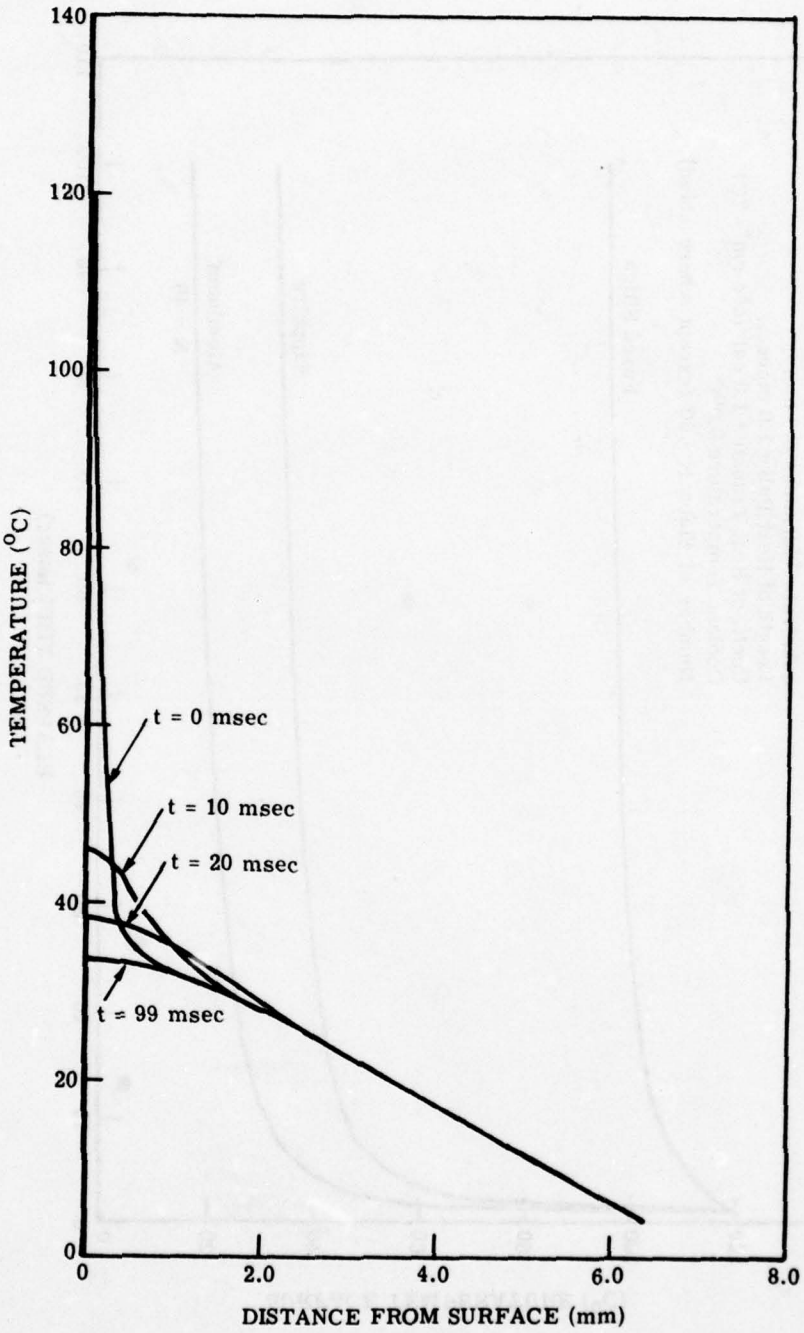

Figure 3. Computed Temperature Distribution Through a 6.3 mm Thick Sapphire Substrate at Several Elapsed Times After the Heat Pulse

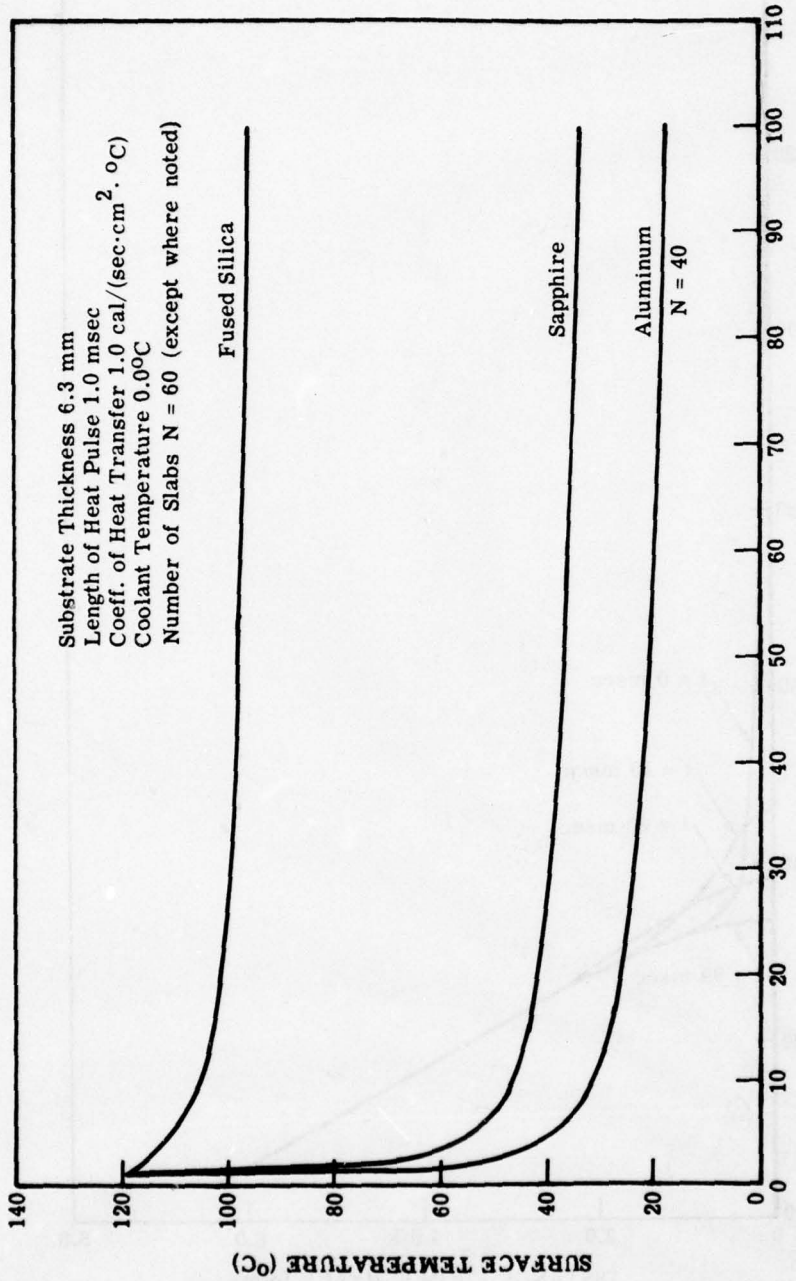

Figure 4. Effect of Substrate Material on the Surface Temperature

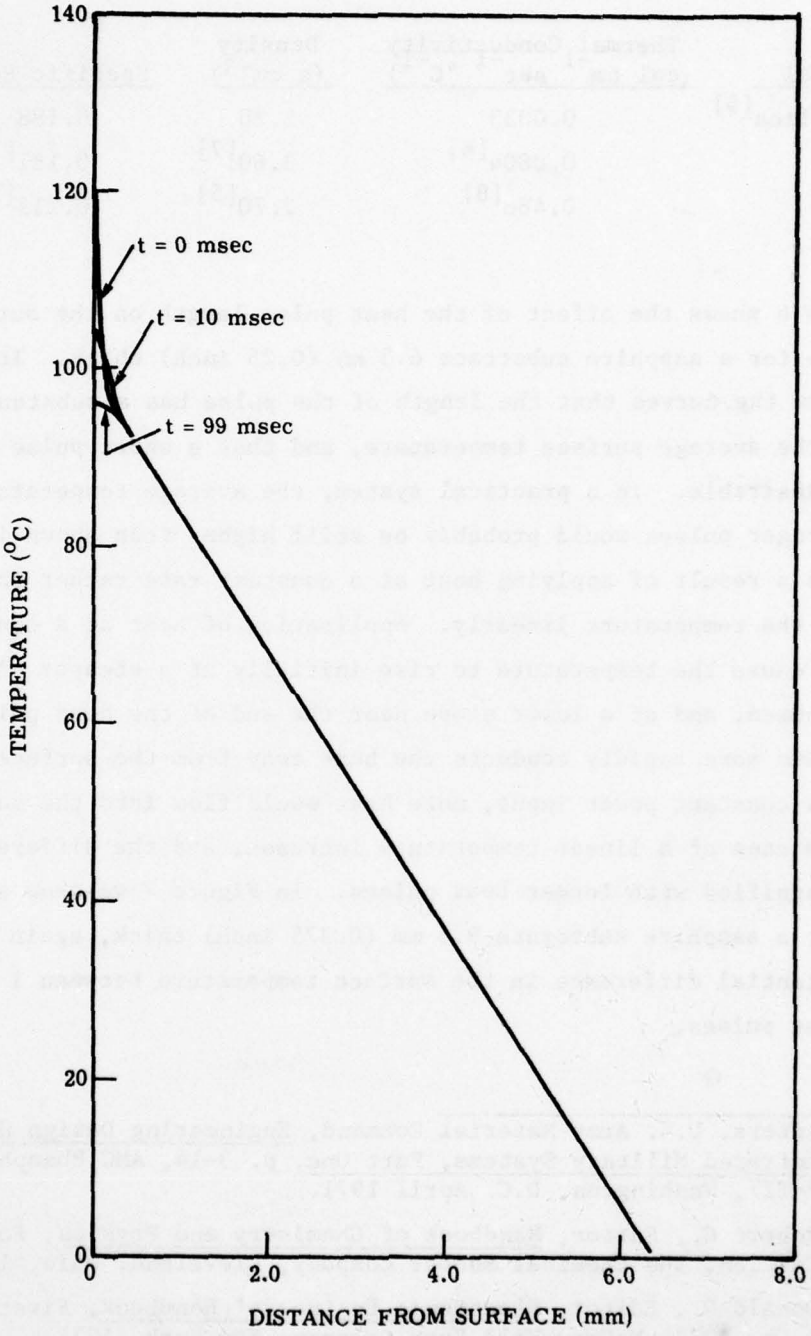

Figure 5. Temperature Distribution Through a 6.3 mm Thick Fused Silica Substrate at Several Elapsed Times After the Heat Pulse

TABLE 1. MATERIAL PARAMETERS

Material	Thermal Conductivity ($cal\ cm^{-1}\ sec^{-1}\ °C^{-1}$)	Density ($g\ cm^{-3}$)	Specific Heat
Fused Silica[5]	0.0033	2.20	0.188
Sapphire	0.0804[6]	3.60[7]	0.181[7]
Aluminum	0.488[8]	2.70[5]	0.215[5]

Figure 6 shows the effect of the heat pulse length on the surface temperature for a sapphire substrate 6.3 mm (0.25 inch) thick. It is evident from the curves that the length of the pulse has a substantial effect on the average surface temperature, and that a short pulse length is desirable. In a practical system, the average temperature with the longer pulses would probably be still higher than shown in Figure 6 as a result of applying heat at a constant rate rather than increasing the temperature linearly. Application of heat at a constant rate would cause the temperature to rise initially at a steeper slope than we assumed, and at a lower slope near the end of the heat pulse as the substrate more rapidly conducts the heat away from the surface. Thus with a constant power input, more heat would flow into the substrate than in the case of a linear temperature increase, and the difference would be magnified with longer heat pulses. In Figure 7 we show similar results for a sapphire substrate 9.5 mm (0.375 inch) thick, again showing a substantial difference in the surface temperature between 1 and 10 msec heat pulses.

5. Headquarters, U.S. Army Material Command, Engineering Design Handbook, Infrared Military Systems, Part One, p. 3-14, AMC Phamphlet No. 706-127, Washington, D.C. April 1971.
6. West, Robert C., Editor, Handbook of Chemistry and Physics, Forty-Ninth Edition, The Chemical Rubber Company, Cleveland, Ohio, 1968.
7. Fink, Donald G., Editor, Electronic Engineers' Handbook, First Edition, p. 6-72, McGraw-Hill Book Company, New York, 1975.
8. McAdams, William H., Heat Transmission, p. 445, McGraw-Hill, New York, 1954.

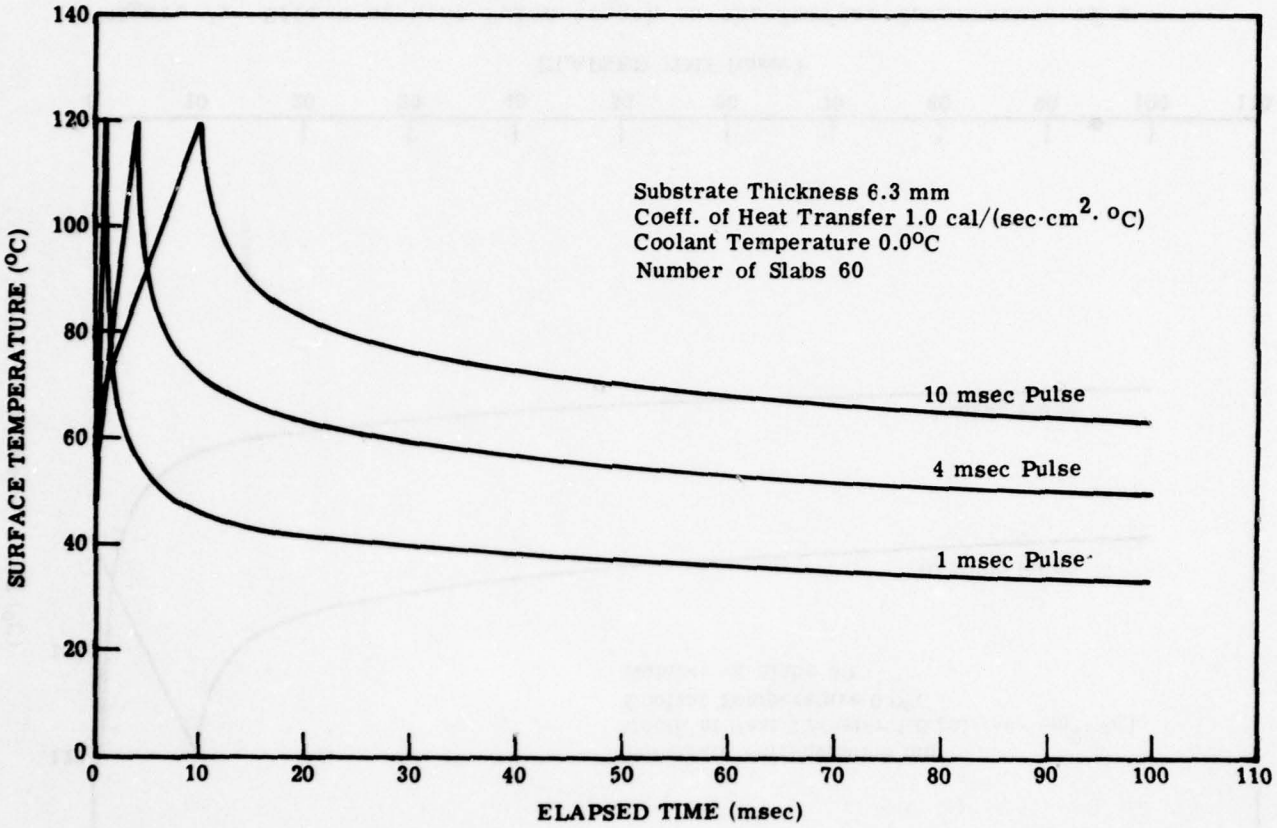

Figure 6. Effect of Heat Pulse Length on the Surface Temperature of a Sapphire Substrate 6.3 mm Thick

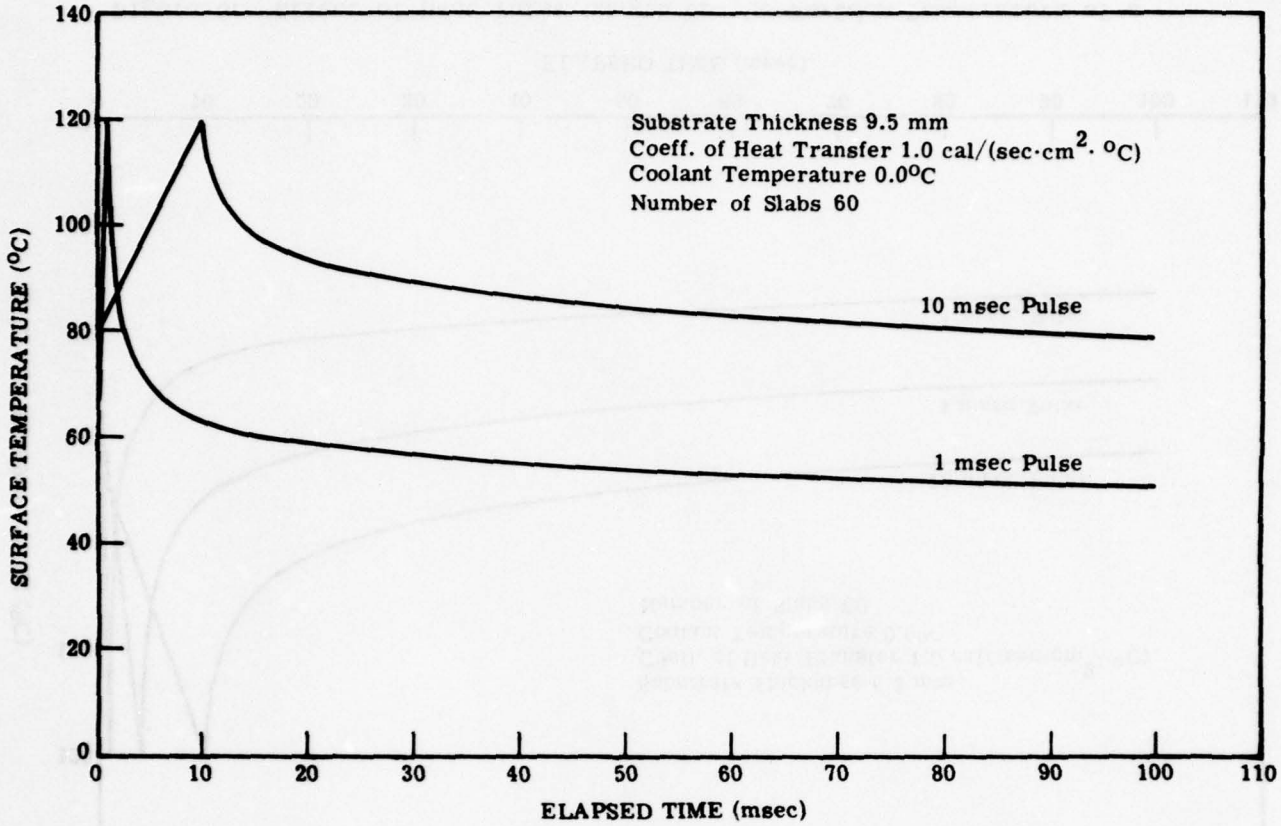

Figure 7. Effect of Heat Pulse Length on the Surface Temperature of a Sapphire Substrate 9.5 mm Thick

The data shown in Figures 6 and 7 clearly indicate the advantages of using short pulses for the thermoplastic heating. A pulse length of 1 msec offers superior performance to a 10 msec pulse, and still shorter pulses would probably lower the average surface temperature even further. For a given heat input, however, reducing the pulse length increases the required power, which not only will increase the complexity of the power supply but also may severely stress, if not destroy, the heating electrode. It might be possible to alleviate the latter problem by redesign of the heating electrode, replacing the transparent conductor with a thick (perhaps opaque) film that can accommodate higher power levels. In light of these considerations, a pulse length of 1 msec appears to be a reasonable compromise, and we accordingly assumed a 1 msec pulse for most of the investigations reported herein.

In Figure 8 we show the effect of the substrate thickness on the surface temperature. Reducing the thickness significantly lowers the average surface temperature since the heat does not need to flow as far. The 3.0 mm substrate thickness is especially effective, with the surface temperature falling to 15° at the end of the cooling period. Although the 3.0 mm thick substrate is therefore attractive, we assumed the 6.3 mm thickness for most of our investigations because we felt that it offers increased rigidity and strength, and that a possible substrate deformation caused by the temperature gradient might be less with the thicker substrate.

Assuming the 6.3 mm sapphire substrate and 1 ms heating pulses, we investigated the effect of the heat transfer coefficient h on the substrate surface temperature (see Fig. 9) for three values of h, 0.1, 1.0, and 2.0 cal/(sec)(cm^2)(°C). Variation of h has considerably less effect on the surface temperature than do changes in the substrate thickness or in the length of the heat pulses; in fact, the change in h from 1.0 to 0.1 only changes the substrate temperature (at the end of the cooling period) from 34° to 41°. This is fortunate since the assumption that h is 1.0 cal/(sec)(cm^2)(°C) is probably unwarranted, and even a value of 0.1 may be optimistic. As mentioned previously, it is difficult to

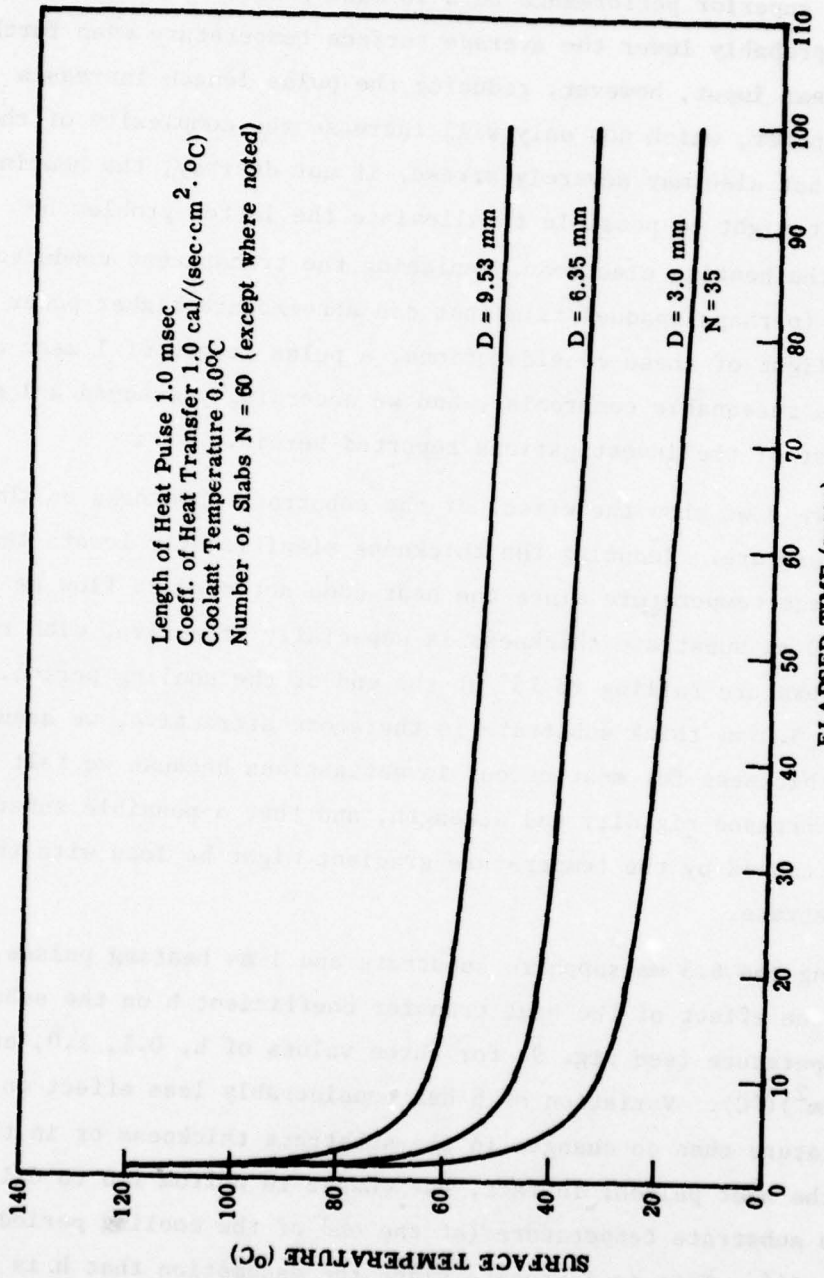

Figure 8. Effect of Substrate Thickness D on the Surface Temperature of a Sapphire Substrate

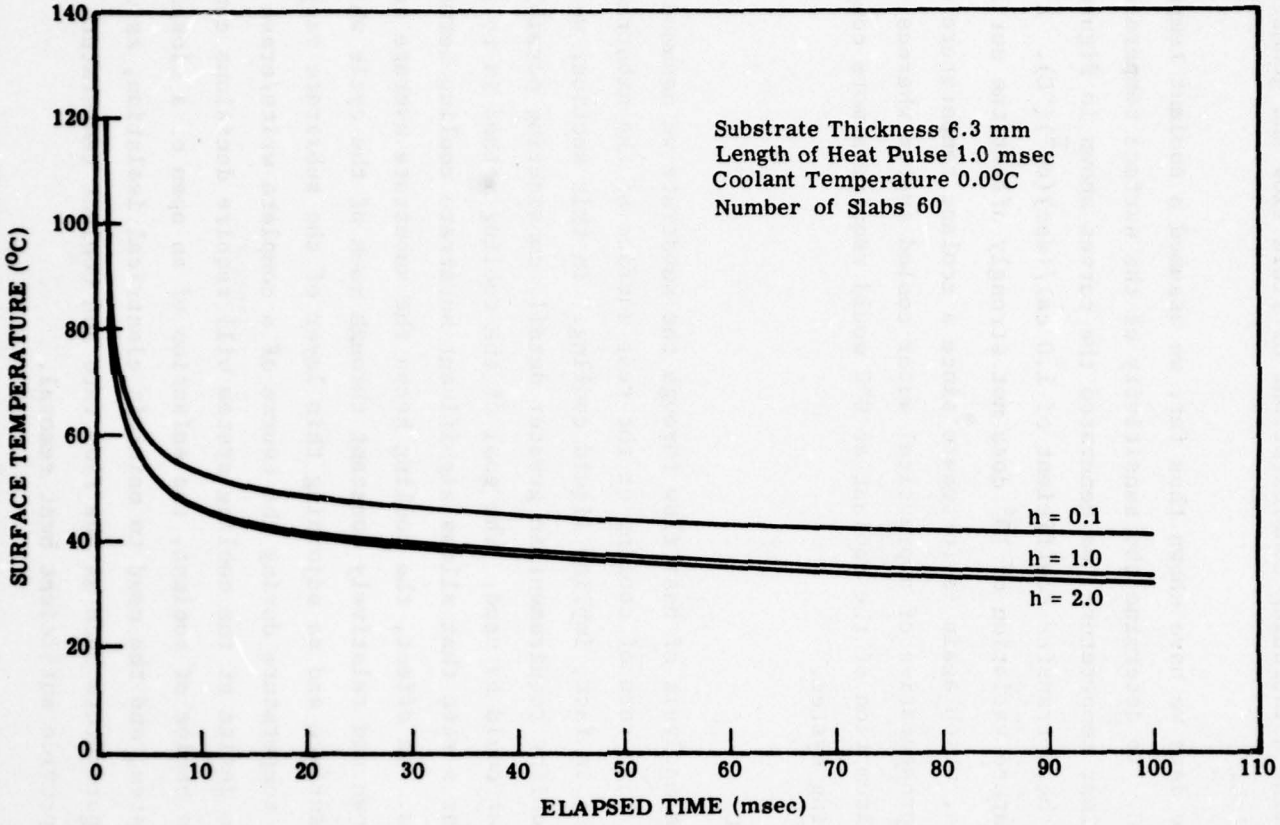

Figure 9. Effect of the Heat Transfer Coefficient h on the Surface Temperature of a Sapphire Substrate

predict a realistic value for h because of the large number of variables that determine h including considerations of fluid flow and geometric configuration.

In the data we have shown thus far, we assumed a coolant temperature of 0°C. To determine the sensitivity of the surface temperature to the coolant temperature, we generated the curves shown in Figure 10 assuming a heat transfer coefficient of 1.0 cal/(sec)(cm^2)(°C). A coolant temperature variation of 10° does not strongly affect the surface temperature, which again is fortunate since a coolant temperature of 10°C is representative of a practical water cooled system whereas the previous assumption of the coolant at 0°C would require a more complicated cooling system.

4. COOLING

In the analysis of heat flow through the substrate we assumed a relatively high rate of cooling at the rear surface of the substrate, a rate that, in fact, implies liquid cooling. In this section, we discuss the cooling requirement in greater detail, considering possible methods that could be used. The goal of the cooling method is to remove heat at a rate that allows significant substrate cooling between heat pulses. In effect, the cooling keeps the substrate average temperature down and relatively constant through much of the cycle while the front surface and an adjoining thin layer of the substrate vary rapidly in temperature during the course of a complete write/erase cycle. The design of the cooling system will require decisions concerning the choice of coolant, the selection of an open or a closed cooling system, and the need to maintain electrical isolation, as well as design parameters such as the flow rate and coolant temperature required to provide sufficient heat removal.

In the absence of experimental data, it is difficult to predict exactly the required rate of heat removal, but we can make an estimate based on the estimated energy needed to heat the thermoplastic in an

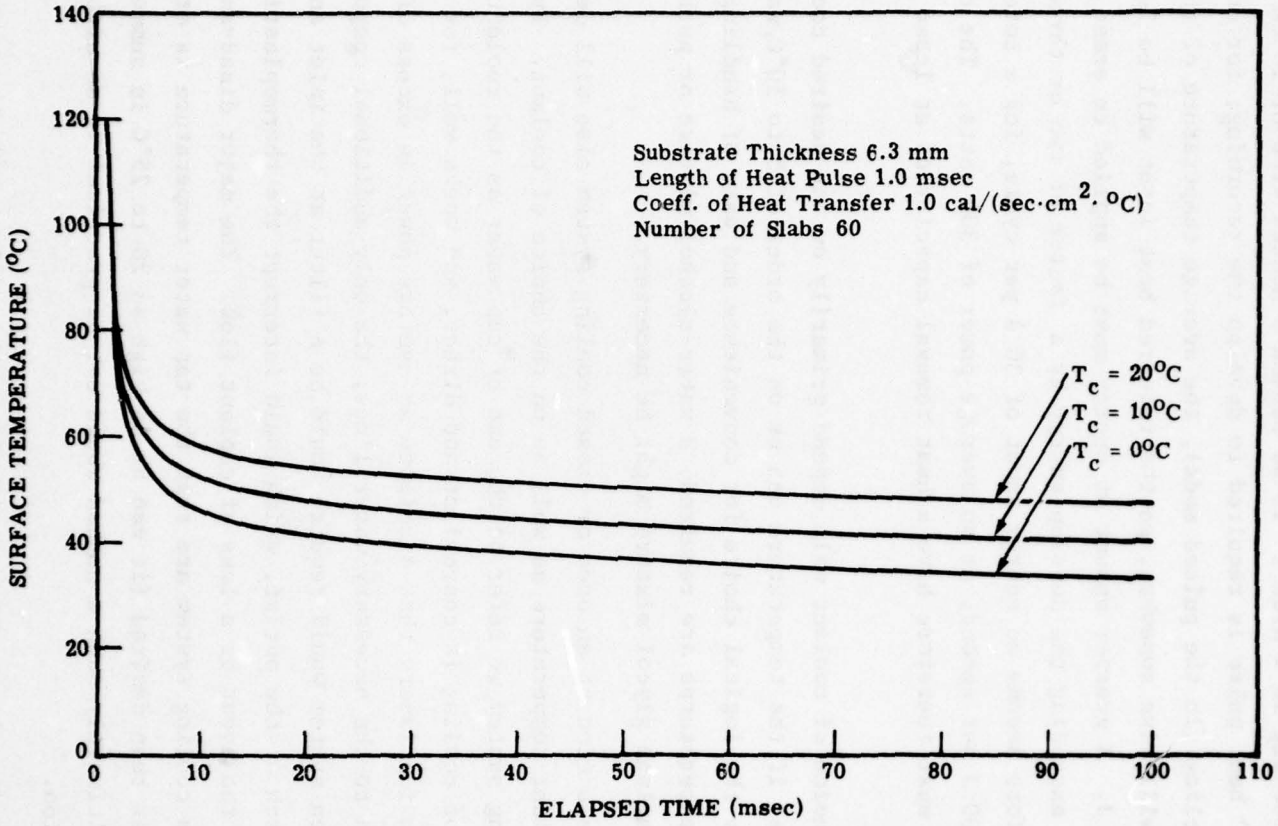

Figure 10. Effect of the Coolant Temperature T_c on the Surface Temperature of a Sapphire Substrate

erase pulse. A typical energy density sufficient to develop a thermoplastic recording is 2 J/cm^2. If we assume a heated area of 10 cm^2, then a 20 J heat pulse is required to develop the recording; for continuous cycling (in the pulsed mode), the average temperature of the substrate will rise somewhat, so the required heat input will be less, perhaps 10 J. A greater amount of energy must be applied to erase the recording, exceeding the develop energy by a factor of two or three. We will therefore assume an energy input of 30 J per cycle, for a total input of 300 J per second, or an average power of 300 watts. The cooling system must therefore have a heat removal capacity of at least 300 watts.

The choice of coolant will depend primarily on the desired coolant temperature: if the temperature can be on the order of 5 to 10°C, water is probably the logical choice for convenience and ease of handling. If lower temperatures are required, a water-alcohol mixture or perhaps a water-ethylene glycol mixture might be necessary.

The selection of an open or closed cooling system also will depend on the coolant temperature as well as on the choice of coolant. By an open cooling system we refer to the use of tap water as the coolant. This mode of cooling is convenient and direct, and works well, for example, with ion lasers that dissipate an average power in excess of 5 kw. In addition to the necessary water lines, the only additional components that an open system would require would be a filter at the inlet and a flow switch at the outlet, which would interrupt the thermoplastic heating in the event of a loss of coolant flow. The major disadvantages of the open cooling system are that the tap water temperature is at times higher than desired (it can be as high as 20 to 25°C in summer), and that ultimately such a method would not be practical in an airborne configuration.

A closed cooling system recirculates the coolant and thus requires a pump and some form of heat exchanger, which may, in turn, use tap water as its coolant. The closed system can reach low temperatures by

including a refrigeration system, and should be capable of maintaining a reasonably constant coolant temperature. In a closed system, the filter would not be necessary, but the flow switch would still be required and a temperature sensor might be added to monitor the coolant temperature. The major disadvantage of the closed cooling system is the complexity and cost of the required components; such a system would, however, be used in an airborne modulator system.

In the existing breadboard modulator, the vacuum housing in the vicinity of the faceplate is maintained at a high voltage level (7 kV) to establish the required potential drop between the electron gun and faceplate. It will therefore be necessary either to provide for electrical isolation of the cooling system, or to redesign the modulator so that the faceplate is at or near ground potential and the gun is at a high negative potential. In the latter case, d-c isolation must be provided between the gun and the incoming modulating signal.

The operating parameters of the cooling system, principally the flow rate and coolant temperature, will depend on the actual rate of heat input to the faceplate, the configuration of the cooling channel in the faceplate, and design choices based on considerations of system complexity and cost. The more effective the cooling system is at maintaining a low surface temperature of the substrate, the lower the average temperature of the thermoplastic will be. Within limits, there will tend to be a tradeoff between a low coolant temperature and a high flow rate.

An alternate approach to cooling the thermoplastic substrate, perhaps to a temperature below that of the tap water, is to place thermoelectric coolers across the rear surface of the substrate. Thermoelectric devices can transfer heat from a cool surface to a warmer surface; the heat must ultimately be removed from the warm surface, however, if a steady heat flow is to be maintained. An open cooling system could presumably be used in turn to remove the heat from the warm surface.

The phenomenon of thermoelectricity is based on three complementary effects named after their discoverers, the Seebeck effect, the Peltier effect, and the Thomson effect. The Seebeck effect is the property that when two materials are joined at two places, and the two junctions are at different temperatures, a current will flow; this is the well-known property of the thermocouple. The Peltier effect is essentially the reverse, that when a current is passed through a junction of two different materials, heat will be absorbed or given off, depending on the direction of the current. The Thomson effect is the property that when the ends of a single piece of material are at different temperatures and a current passes through the material, heat is absorbed or given off, again according to the direction of the current. As might be expected from their complementary nature, these effects are related to one another. For thermoelectric cooling we are interested primarily in the Peltier effect (detailed discussion on this and the other effects can be found in Refs. 9 and 10).

We will briefly indicate the salient features of a thermoelectric cooler and estimate the cooling capacity of a cooler that has typical device characteristics. Following the development given in Heikes and Ures[11], we will consider heat removal with the thermoelectric couple shown schematically in Figure 11. The couple is formed by joining two thermoelectric materials with a good electrical and thermal conductor at the temperature T_c. With the current flow as shown, the device pumps heat from the cool reservoir at T_c to the warm reservoir at temperature T_h. Because the arms of the device connect the warm and cool reservoirs, they should have a low thermal conductivity since heat will be conducted in the direction opposite to that of the heat pumping. The thermoelectric materials that constitute the arms are usually semi-

9. Heikes, Robert R. and Ures, Roland W., Jr., Thermoelectricity: Science and Engineering, Interscience Publishers, New York, 1961.

10. Egli, Paul H., Editor, Thermoelectricity, John Wiley & Sons, New York, 1960.

11. Heikes, Robert R. and Ures, Roland W., Jr., Thermoelectricity: Science and Engineering, Chapt. 15, Interscience Publishers, New York, 1961.

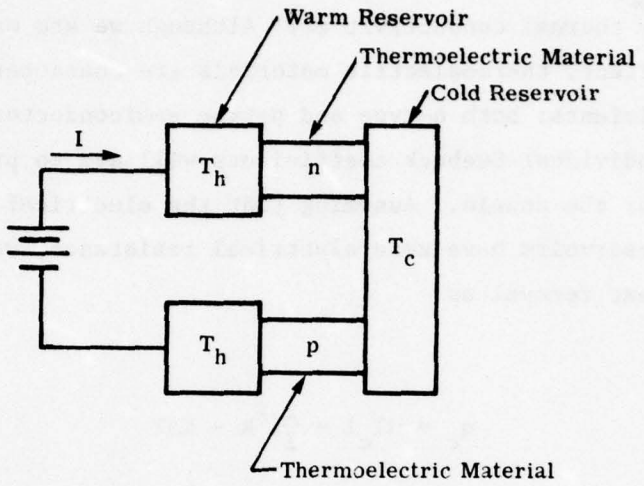

Figure 11. Schematic Configuration of a Thermoelectric Couple

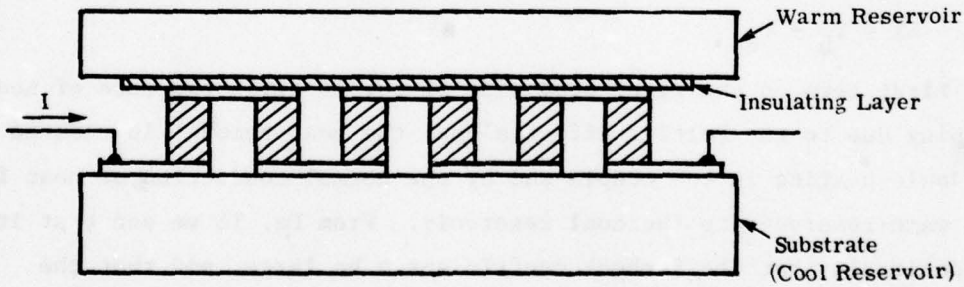

Figure 12. Configuration of a Thermoelectric Cooler Using Multiple Couples

conductors, which form an effective thermoelectric couple, but have relatively low thermal conductivities. Although we are making use of the Peltier effect, thermoelectric materials are characterized by their Seebeck coefficients; both n-type and p-type semiconductors are used since their individual Seebeck coefficients will add to provide a higher coefficient for the couple. Assuming that the electrical conductors at the heat reservoirs have zero electrical resistance, we can express the rate of heat removal as

$$q_c = \alpha T_c I - \frac{1}{2} I^2 R - K\Delta T \qquad (15)$$

where α = Seebeck coefficient of the couple

T_c = temperature of the cool reservoir (°K)

I = current

R = series resistance of the thermoelectric materials

K = thermal conductance of the thermoelectric materials

$\Delta T = T_h - T_c$

The first term on the right hand side of Eq. 15 gives the rate of heat pumping due to the Peltier effect alone; the heat removal is reduced by Joule heating in the couple and by the normal conduction of heat from the warm reservoir to the cool reservoir. From Eq. 15 we see that it is desirable that the Seebeck coefficient α be large, and that the electrical resistance R, the thermal conductance K, and the temperature differential ΔT all be small. The Seebeck coefficient of the couple is defined as

$$\alpha = \alpha_p - \alpha_n \qquad (16)$$

where α_p is the Seebeck coefficient of the p-type material and α_n is the

coefficient of the n-type material. The thermal conductance is given by

$$K = k_n b_n + k_p b_p \tag{17}$$

where k is the thermal conductivity of the respective material and b is the ratio of the cross section area to the length of the material. Similarly

$$R = \frac{\rho_n}{b_n} + \frac{\rho_p}{b_p} \tag{18}$$

where ρ is the resistivity of the thermoelectric material. It can be shown[11] that the maximum heat pumping rate is

$$q_c' = \frac{\alpha^2 T_c^2}{2R} - K\Delta T \tag{19}$$

In order to form an estimate of the cooling capacity of a thermoelectric couple, we can determine q_c' for a device made by joining two thermoelectric materials that have parameters typical of the materials used for thermoelectric cooling. The materials parameters are given in Table 2. Ignoring contact resistance and solving for q_c' gives a value of 36 watts/couple. Because of the small size of a couple, many couples would be placed along the rear surface of the substrate as indicated in Figure 12. In our example, the area of each arm is about 0.3 cm^2. The couple has two arms, and typically the arms are separated by a distance similar to their diameter. In an array such as that indicated by Figure 12, each couple might occupy approximately 2 cm^2, so

TABLE 2. THERMOELECTRIC MATERIALS PARAMETERS USED IN THE EXAMPLE
(Parameters obtained from Ref. 11)

$\alpha_p = -\alpha_n = 230\ \mu v/°C$
$\rho_n = \rho_p = 10^{-3}\ \Omega \cdot cm$
$k_n = k_p = 0.015$ watts/(°C)(cm)
length of arms = 3.2 mm
area of arms = 32 mm^2
$T_c = 273°K$
$T_h = 293°K$

that as many as 50 couples could be located on the rear surface of the substrate, corresponding to the 100 cm^2 heated area. It would appear, therefore, that the cooling capacity of the thermoelectric cooler is adequate. At the maximum heat pumping rate given by Eq. 19, the current is[11]

$$I = \frac{\alpha T_c}{R} \tag{20}$$

Using the parameters given in Table 2, the current required is 628 amperes. This current level can be reduced by using thermoelectric arms that have a smaller cross sectional area, which will also reduce both the maximum heat pumping rate and the area required by each couple.

Since heat must be removed from the warm reservoir at the same rate at which it is pumped from the cool reservoir and generated through Joule heating, there will be a need for additional cooling at the warm reservoir. The thermoelectric cooler, however, would permit cooling of the substrate to temperatures below that of the coolant used to remove heat from the warm reservoir. Thermoelectric cooling may also provide better temperature control at the substrate since fluctuations in the

coolant temperature could be compensated by changes in the heat pumping rate. Presently available T-E cooler modules fall short of projected heat flux requirements by about an order of magnitude.

5. FACEPLATE CONFIGURATION

From the results of the thermal analyses, we can develop a faceplate configuration that should permit continuous thermoplastic cycling at rates of up to 10 cycles per second. The faceplate will include a thermoplastic substrate that has a high thermal conductivity and a cooling channel at the rear surface of the substrate to permit liquid cooling. The substrate should be sapphire with a nominal thickness of 6.3 mm (0.25 inch) and with a writing area that is a square with a nominal dimension of 25 mm; to provide for a uniform thermoplastic temperature over the entire writing area, it may be necessary to heat a larger area to reduce or eliminate edge effects. The substrate diameter, therefore, will be in the vicinity of 50 to 75 mm. A special mounting plate will be required to mate the substrate to the existing modulator, which currently uses substrates of 125 mm diameter. The mounting plate design must accommodate the average temperature variation of the substrate while maintaining the integrity of the vacuum envelope.

Because of phase perturbations caused by heating of the coolant, transmissive readout appears to be impractical. The thermoplastic must, therefore, be read out in reflection from the vacuum envelope. Since the reflection coefficient of the thermoplastic surface is relatively low, the intensity of the diffracted signal will be low and it will be important to minimize optical noise, including reflections from surfaces other than the free surface of the thermoplastic. The extent to which such reflections will be significant will be a function of the final design of the faceplate: if, for example, the heating electrode between the thermoplastic and the substrate is highly absorbing, reflections from the rear surface of the substrate or from surfaces that form the cooling channel will be insignificant. If the reflections are significant, it may be necessary to provide anti-reflection coatings on certain surfaces, in particular the rear surface of the substrate. Other

methods of reducing surface reflection noise in the signal region include adding an absorbing dye to the thermoplastic, adding a dye to the coolant, providing anti-reflection coatings on the rear plate of the cooling channel, or tilting the rear plate. Figure 13a shows a sketch of a possible faceplate design with a substrate coated on the front surface with the heating electrode and the thermoplastic layer, and a cooling channel formed by locating a second plate, which can be glass or metal, as shown. The rear plate is shown tilted slightly to remove reflections from the optical system; a tilt of several degrees should be sufficient to separate the reflections from the diffracted signal.

It may be desirable to add a thin layer having a low thermal conductivity between the thermoplastic and the substrate, as shown in Figure 13b. The purpose of this layer would be to reduce the rate of heat flow into the substrate during the very short heat pulse, yet not greatly reduce the rate at which the heat flows out of the thermoplastic between heat pulses. Reducing the heat flow into the substrate during the heat pulse should reduce the power requirements placed on the electronics, and should also reduce the total heat flow into the substrate over the course of one cycle period. The requirements on the layer are that it be compatible with both the substrate and the heating electrode, and that it have sufficient thickness (it probably should be comparable to the thermoplastic thickness) with the required surface quality. In addition, if the insulating layer absorbs the transmitted light, it would help to reduce the surface reflection problem. It should not, however, cause strong reflections itself due to a large index mismatch at either surface. In Figure 13b, the additional layer is assumed to be absorptive to eliminate the reflection problem, and the rear plate is shown parallel to the substrate.

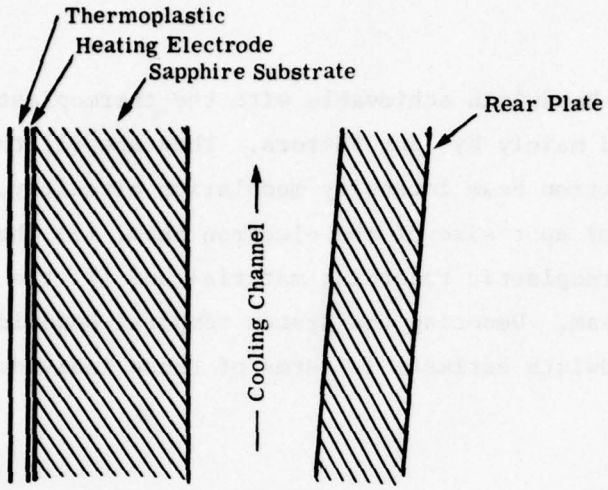

(a) Possible faceplate configuration with rear plate slightly tilted to offset reflection.

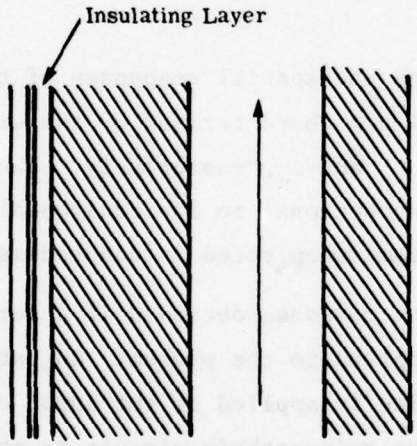

(b) Possible faceplate configuration including an insulating layer between the thermoplastic layer and the heating electrode.

Figure 13. Possible Faceplate Configurations for Rapid Modulator Cycling

SECTION III
RECORDING BANDWIDTH

1. INTRODUCTION

The temporal bandwidth achievable with the thermoplastic modulator system is governed mainly by four factors. They are (1) the video response of the electron beam intensity modulation circuitry, (2) the spatial response or spot size of the electron beam, (3) the spatial response of the thermoplastic recording material and (4) the sweep speed of the electron beam. Denoting the system temporal bandwidth as B we can express a bandwidth estimate in terms of these individual factors as

$$B = \frac{1}{2\left[\rho_s^2 + \frac{\rho_b^2}{V^2} + \frac{\rho_m^2}{V^2}\right]^{1/2}} \qquad (21)$$

The electron beam modulation and the spatial responses of the electron beam and the recording material are characterized by the width of their impulse response functions ρ_s, ρ_b and ρ_m, respectively. The bandwidth of each of these elements is proportional to the reciprocal of the impulse response width. The writing beam sweep speed is denoted as V.

The impulse response is the response obtained if a very short pulse, ideally a delta function, is applied to the system. In particular, if a delta-function-like video pulse is applied at the input of the amplifier that feeds the electron gun grid-cathode circuit to modulate the electron beam current, the resultant beam current pulse will represent the impulse response for the beam intensity modulation. The width of the current pulse, measured at fifty percent of its maximum value, is the measure of the response function ρ_s used in the above expression for system bandwidth. Similarly the writing beam spatial impulse response is the charge distribution deposited by the scanning electron beam when

its current is a very short, or delta-function-like, pulse. The width of the charge distribution at the fifty percent level in the scan direction is ρ_b. The thermoplastic recording material impulse response width ρ_m corresponds to the recorded deformation width obtained when the charge distribution deposited by the writing electron beam is again very narrow. The bandwidth of each of these elements at fifty percent frequency response is one half the reciprocal of the impulse response width.

The expression for system bandwidth B indicates the familiar facts that in order to maximize B we (1) minimize ρ_s, (2) minimize ρ_b and ρ_m and (3) maximize the sweep speed V.

The sweep speed will have an upper bound dictated by separate considerations in the recording process, namely the recording material sensitivity and the recording format size. The recording sensitivity of the thermoplastic material is a measure of the charge required to realize the desired depth of deformation of the thermoplastic. Denoting the minimum required exposure in charge per unit area as E and the writing electron beam density in charge per unit area per second as J, we have the following expression for the write beam exposure constraint

$$E = \frac{J\rho_b}{V} \qquad (22)$$

Thus, given E, J and ρ_b, the sweep speed V must be constrained to a value low enough to satisfy the recording material exposure requirement. In addition, although typically a secondary consideration, sweep speed must be limited if the available area of the recording material and the recording format are prescribed.

2. PREVIOUS PERFORMANCE

A system temporal bandwidth of 40 MHz at fifty percent response has been achieved with the experimental thermoplastic modulator bread-

board[12]. Recording response was realized up to 100 MHz, but at a level considerably below fifty percent. The response parameters realized in the modulator design were as follows:

Write beam intensity modulation	$\rho_s = 8 \times 10^{-9}$ sec
Write beam spatial response	$\rho_b = 17 \times 10^{-3}$ mm
Thermoplastic spatial response	$\rho_m = 10 \times 10^{-3}$ mm
Sweep speed	$V = 2 \times 10^{6}$ mm/sec

The recording sensitivity E for an eight micron thermoplastic layer was about 10^{-11} coulombs/mm^2 for a 10^{-4} mm deformation depth. A writing beam current of 4×10^{-7} A provided a current density of 1.4×10^{-3} amp/mm^2 which was suitable for deformation depths to about 10^{-4} mm with a single sweep exposure at a sweep speed of 2×10^{6} mm/sec. This range of deformation depth is appropriate for the intended linear mode of operation of the thermoplastic modulator as an input to a coherent optical processor.

3. BANDWIDTH ENHANCEMENT

Enhanced temporal frequency response over that previously achieved with the thermoplastic modulator can be realized with available technology. Increased performance over a 100 MHz bandwidth can be obtained through improvements in the beam intensity modulation and the writing beam and recording material spatial responses. A 100 MHz bandwidth at fifty percent response can, of course, be achieved in a varity of individual component responses. As a nominal working goal we used the set of component impulse response parameters listed below while retaining the previous sweep speed of 2×10^{6} mm/sec.

Write beam intensity modulation	$\rho_s = 3 \times 10^{-9}$ sec
Write beam spatial response	$\rho_b = 7 \times 10^{-3}$ mm
Thermoplastic spatial response	$\rho_m = 4 \times 10^{-3}$ mm

12. Cindrich, I., Currie, G., and Leonard, C., "A Thermoplastic Input Data Modulator for Real-Time Processing of SAR Data," Proceedings of the Technical Program, Electro-Optical Systems Design Conf.-1975, pp. 301-309, November 1975.

These individual impulse response widths correspond to a beam intensity bandwidth of 70 c/mm and a recording material bandwidth of 130 c/mm. On a cascaded basis through the modulator components we would realize 167 MHz bandwidth in beam current intensity modulation; 108 MHz bandwidth in writing beam exposure at the recording material surface; and 100 MHz in recorded deformation modulation at the thermoplastic surface.

Using a 25 mm scan line length with the 2×10^6 mm/sec scan speed results in 1250 recorded cycles of 100 MHz video signal along a scan line for a time-bandwidth product of 1250. In the orthogonal dimension, the recorded line width of 8.7×10^{-3} mm given by the combined writing beam and thermoplastic spatial responses provides a space-bandwidth product of 1445 over a 25 mm raster width. The two-dimensional space-bandwidth product over the 25 × 25 mm area is thus 1.8×10^6. It should be noted that a 50 mm × 50 mm recording area is actually available with the present modulator design which would provide a fourfold increase in the two dimensional space-bandwidth product, increasing it to 7.2×10^6.

4. WRITING BEAM MODULATION

Modulation of the write beam current is accomplished by control of the cathode-grid voltage of the electron gun structure as depicted in the schematic diagram of Figure 14. The beam current is approximately linearly proportional to the cathode-grid voltage v. The linear relationship is given by the expression

$$i = K_b v \tag{23}$$

with $K_b \simeq 2.5 \times 10^{-8}$ amp/volts

Of primary interest to the beam current modulation bandwidth is the

relationship between cathode-grid voltage v and the input signal s*. Figure 15 provides an equivalent circuit diagram useful in relating v to s. The video amplifier is characterized as a voltage source with voltage gain K_s and internal impedance Z_1. The coaxial transmission line of length l and characteristic impedance Z_0 has voltage v_1 at its input and v_2 at its output end. The coaxial line is terminated in the complex impedance Z_2 which consists of a shunt resistor R used for impedance matching, the inductance L of the wire leads within the electron gun envelope, and capacitance C between the cathode and grid-one. The expression for v as a function of s, in the frequency domain, will be described stepwise from the input to the output. Capital letters will be used for the frequency domain expression of signal variables.

The video amplifier establishes the voltage v from the input s as

$$v_0 = K_s s \tag{24}$$

With the coaxial line of characteristic impedance Z_0 and the video amplifier source impedance Z_1, the voltage input V_1 to the coaxial line is

$$V_1 = \frac{Z_0}{Z_1 + Z_0} K_s S \tag{25}$$

For the matched condition,

$$V_1 = \frac{SK_s}{2} \tag{26}$$

*Although transit time of the electron beam from cathode to grid one can affect modulation bandwidth, this effect is negligible for frequencies of interest here.

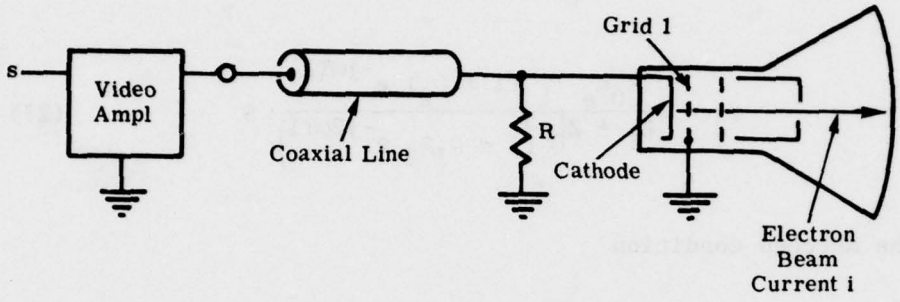

Figure 14. Electron Beam Modulation

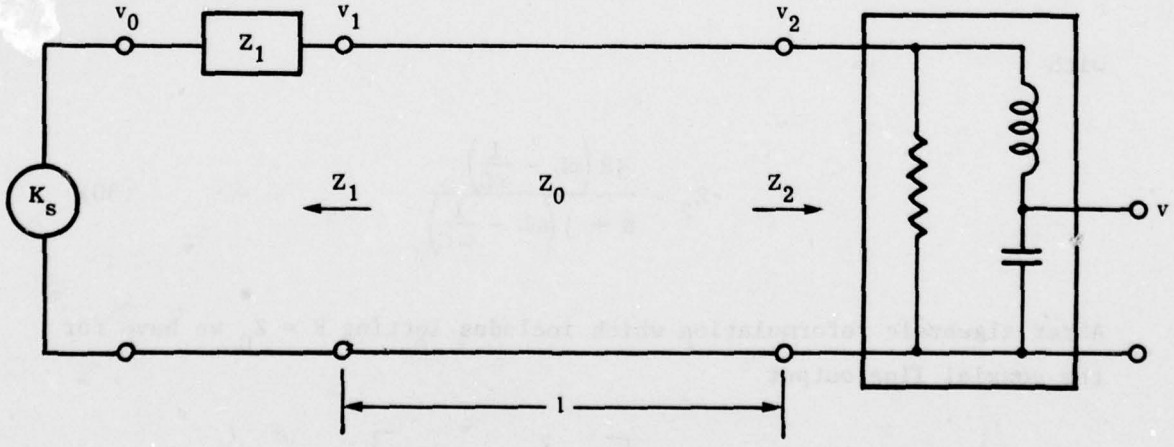

Figure 15. Equivalent Circuit for Cathode-Grid Modulation

The coaxial line output V_2 when loaded with the impedance Z_2, with input and output reflection coefficients ρ_1 and ρ_2 and the line constant T, is

$$V_2 = \left(\frac{Z_0 K_s}{Z_1 + Z_0}\right) \frac{(1 + \rho_2)\ e^{-j\omega T1}}{\left(1 - \rho_1 \rho_2\ e^{-j2\omega T1}\right)} \cdot S \tag{27}$$

and for the matched condition

$$V_2 = \frac{K_s}{2}(1 + \rho_2)\ e^{-j\omega T1} \cdot S \tag{28}$$

The reflection coefficient ρ_2 at the coaxial line output has the form

$$\rho_2 = \frac{Z_2 - Z_0}{Z_2 + Z_0} \tag{29}$$

with

$$Z_2 = \frac{jR\left(\omega L - \frac{1}{\omega C}\right)}{R + j\left(\omega L - \frac{1}{\omega C}\right)} \tag{30}$$

After algebraic reformulation which includes letting $R = Z_0$ we have for the coaxial line output

$$V_2 = \frac{K_s\ e^{-j\omega T1}}{2}\left[\frac{2j\left(\omega L - \frac{1}{\omega C}\right)}{Z_0 + 2j\left(\omega L - \frac{1}{\omega C}\right)}\right] \cdot S \tag{31}$$

Finally, we have the cathode-grid output V as a function of V_2 given by the impedance divider relation

$$V = \frac{-j\frac{1}{\omega C}}{j\left(\omega L - \frac{1}{\omega C}\right)} V_2 \tag{32}$$

$$V = K_s\, e^{-j\omega T1}\left[\frac{-j\frac{1}{\omega C Z_0}}{1 + 2j\left(\omega\frac{L}{Z_0} - \frac{1}{\omega C Z_0}\right)}\right] \cdot S \tag{33}$$

The grid-cathode voltage (and beam current) as a function of the input to the video amplifier is given by Eq. 33. This expression consists of the fixed gain constant K_s, a distortionless phase shift $\omega T1$ caused by the transmission time delay through the coaxial line, and the frequency response function given by the bracketed term which we will denote $A(\omega)$ for convenience. Briefly, $A(\omega)$ has essentially constant magnitude and zero phase for frequencies from $f = 0$ to $f \simeq \frac{1}{2\pi}\sqrt{\frac{1}{LC}}$. For frequencies $f \geq \frac{1}{2\pi}\sqrt{\frac{1}{LC}}$ the magnitude of $A(\omega)$ decreases at -12 dB per octave and the phase is in a transition from zero degrees to -180°.

The bandwidth of the electron beam modulation at fifty percent response, B_s, is given by

$$B_s = \frac{1}{5}\sqrt{\frac{1}{LC}} \tag{34}$$

For bandwidth improvement the most readily accomplished modification to the previous design is the reduction of the inductance L by shortening

the length of the wire lead that gives rise to L. This lead length was approximately 25 cm; reduction by a factor of eight to about 3 cm is reasonable given the scope of the present program. With a factor of eight reduction in L the intensity modulation bandwidth becomes

$$B_s = \frac{1}{5}\sqrt{\frac{1}{LC/8}}$$

$$\simeq \frac{2.8}{5}\sqrt{\frac{1}{LC}} \qquad (35)$$

The factor of 2.8 increase in bandwidth would allow an improvement from the previous 62 MHz to about 170 MHz, which is consistent with the nominal goal noted above for the electron beam intensity modulation.

5. WRITE BEAM SPATIAL RESPONSE

The write beam spatial response is described by the electron beam current distribution (cross section) which we denote as $h_b(x, y)$ and its width ρ_b. In the spatial frequency domain we identify the spatial frequency response function $H_b(\omega_x, \omega_y)$ which is just the Fourier transform of $h_b(x, y)$.

We continue our discussion with reference to the spatial domain of h_b (and ρ_b). The beam realized at the recording surface is a magnified version of the beam as it exists in the region between the first and second grids of the electron gun. Typically the aperture in the second grid serves to reduce the beam cone (divergence) angle and is the smallest aperture in the electron gun system. For the large beam deflection angle ($\geq 20°$) utilized, a magnification of about one is most often used. Demagnification is of course a most appropriate approach to realize a smaller spot size while retaining the beam current level. In addition a further reduction in the size of the limiting aperture of the second grid may be implemented, often, however, at some reduction in beam current.

Demagnification by a factor of two along with a decrease in the second grid aperture from the present 25 μm is recommended. A spot size in the range of four to six microns is potentially achievable with this approach. The incorporation of demagnification with low aberration over a 20° deflection angle will require a careful electron optics design and fabrication. Though not readily available a design of this type is believed to have been developed recently by Tarnowski of Image Graphics, Inc.

6. THERMOPLASTIC SPATIAL RESPONSE

The spatial response of the thermoplastic, when approximated as a linear function, can be characterized by the spatial impulse response function $h_m(x, y)$ (the thermoplastic deformation distribution) and its corresponding width ρ_m. The impulse response h_m is defined as the deformation response to an electron beam spot which is very narrow or delta-function-like.

We want a smaller ρ_m which can be achieved to some extent by use of a thinner thermoplastic layer. In the past a thermoplastic layer of 5 μm to 10 μm has been used. The expected amount of change of ρ_m with decreased film thickness is not known and would have to be established by experimental investigation.

Two effects will enter into determining the bound on the lowest value of film thickness. They are electron penetration into the thermoplastic film and the amount of deformation required to achieve adequate signal modulation.

It is expected that film thickness down to about one micron would be admissible which will likely provide a significant reduction in ρ_m or, equivalently, an increase in spatial frequency bandwidth. However, the characteristic of deformation modulation response is such that as bandwidth is increased it is also shifted away from zero frequency. That is the d.c. and very low spatial frequency response is diminished somewhat. This effect can be compensated either by spectral weighting

of the input signal to be recorded or by employing a carrier frequency on the input signal to shift it into the region of best response of the thermoplastic modulator.

SECTION IV
RECORDING DUTY CYCLE

A rectangular raster recording format is used in the thermoplastic modulator. Data is recorded while the electron beam is scanned at a constant speed in one direction. A rapid retrace is performed to return the beam to the start position of the next adjacent scan. The beam is moved at a much slower rate in the direction orthogonal to the scan line to build up the two dimensional raster. The beam position in the scan direction as a function of time is depicted in Figure 16 for a single scan and retrace. To maximize the percent of time available for recording data the duty cycle D must be maximized, where D is defined in terms of the scan time T_s and the retrace time T_r as

$$D = \frac{T_s}{T_s + T_r} \tag{36}$$

The magnetic deflection system used for electron beam scanning currently provides a sweep time of about 12 μsec and a retrace time of similar length.

An increase in duty cycle can be realized by increasing the sweep time T_s and/or decreasing the retrace time T_r. Though an increase in T_s will improve the duty cycle it will cause a lower sweep speed V which impacts on the system temporal bandwidth performance. Recall that the bandwidth B was

$$B = \frac{1}{2\left[\rho_s^2 + \frac{\rho_b^2}{V^2} + \frac{\rho_m^2}{V^2}\right]^{1/2}} \tag{37}$$

Note that the combined write beam and recording material impulse responses are scaled by the sweep speed V such that a reduction in sweep speed

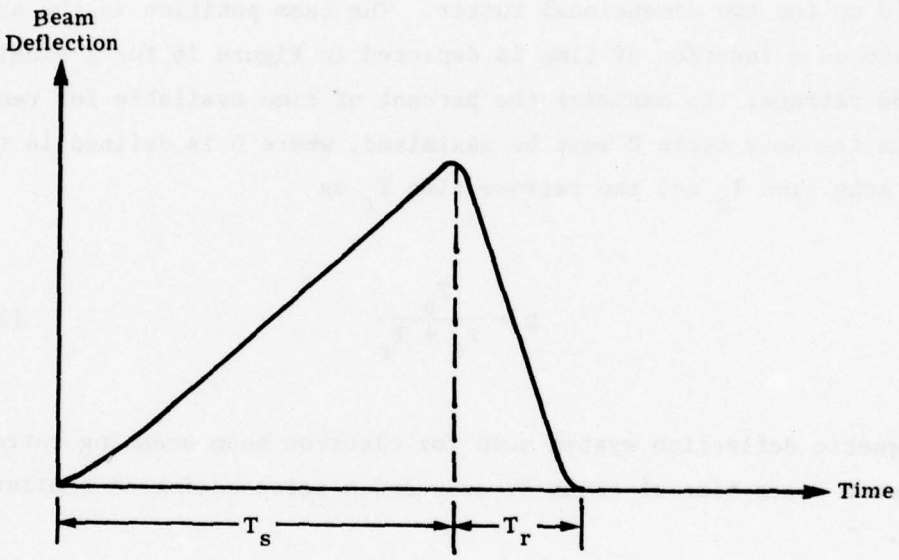

Figure 16. Beam Position in the Rapid Scan Direction as a Function of Time

with unchanged values for ρ_b or ρ_m would reduce the system bandwidth. Thus an increase in sweep time requires that the quantity $\left(\rho_b^2 + \rho_m^2\right)^{1/2}$ be reduced by the same percentage as the sweep speed. Such a reduction of ρ_b and ρ_m would provide another benefit, that of increased data storage density, i.e., a larger space-bandwidth product capability. Small ρ_b can be realized with a new electron gun design in which a reduced electron optic aperture is used and greater demagnification is incorporated in the electron optic lens of the electron gun. Rather than modifying the existing gun structure for this purpose, we would recommend adapting current advanced electron gun designs to the thermoplastic modulator system. A smaller ρ_m for the thermoplastic recording material is expected to be achievable by use of a thinner plastic layer, although this consideration is already included in the component performance goals cited previously in Section III.

The reduction of retrace time T_r can be achieved by increasing retrace speed v_r. The basic considerations relating to a change of v_r will be described here. Beam position is proportional to current in the deflection coil or yoke. We can express position (y) as

$$y = K_y I \tag{38}$$

with K_y = 25 mm/ampere for a coil having an inductance $L \simeq 10^{-4}$ henries. The beam speed during retrace will be

$$v_y = \frac{dy}{dt} = K_y \frac{dI}{dt} \tag{39}$$

For the application of interest here we have a retrace path length of 25 millimeters for which we will take as a goal a retrace time $T_s = 0.25 \times 10^{-6}$ sec, or $v_r = v_y = 10^8$ mm/sec. This low retrace time would provide a duty cycle D ≃ 97%.

The important demands on deflection circuit design are evident from the resultant rate of change of current through the deflection coil and the voltage necessary to provide this current. The rate of change of current will be

$$\frac{dI}{dt} = \frac{v_y}{K_y} = 4 \times 10^6 \text{ amp/sec} \qquad (40)$$

The voltage V required across the coil to provide 4×10^6 amp/sec in a 10^{-4} henry deflection coil is

$$V = L\frac{dI}{dt} = 400 \text{ volts} \qquad (41)$$

The use of a coil with much less than 10^{-4} h inductance would reduce this voltage requirement, but it is not recommended because the coil would likely provide a deflection field of questionable quality (uniformity) due to the small number of coil turns and it would increase the current requirements.

Design of deflection circuitry which incorporates a 400 volt drive and operates with a fractional microsecond retrace is quite demanding. Three design approaches that have been considered are shown in Figure 17. Figure 17a shows a resonant recovery retrace in which a capacitor is switched into the yoke circuit for retrace. An oscillation occurs in which the yoke energy associated with one end of the scan is transferred to the capacitor and then is returned from the capacitor to the yoke with an opposite current polarity, thus causing retrace. At the end of the retrace the normal scan drive circuit takes over. Although one high voltage transistor is required for this circuit arrangement, it does not pass the yoke current during the high voltage retrace, and

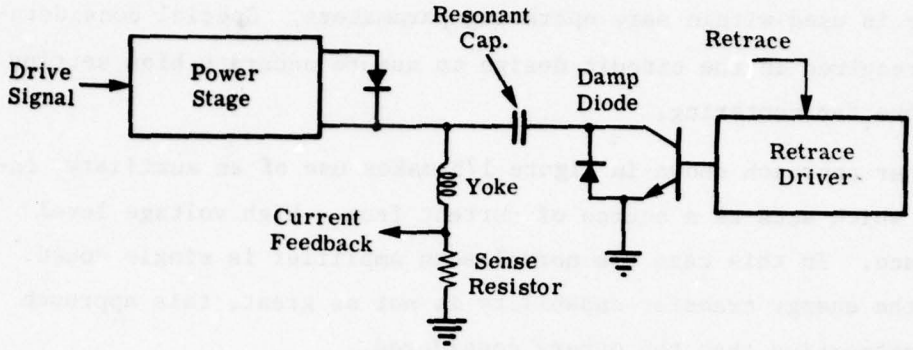

(a) Resonant retrace.

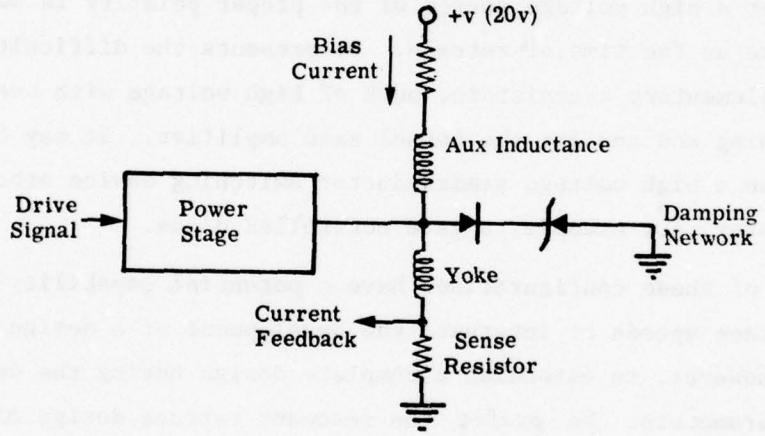

(b) Inductive retrace.

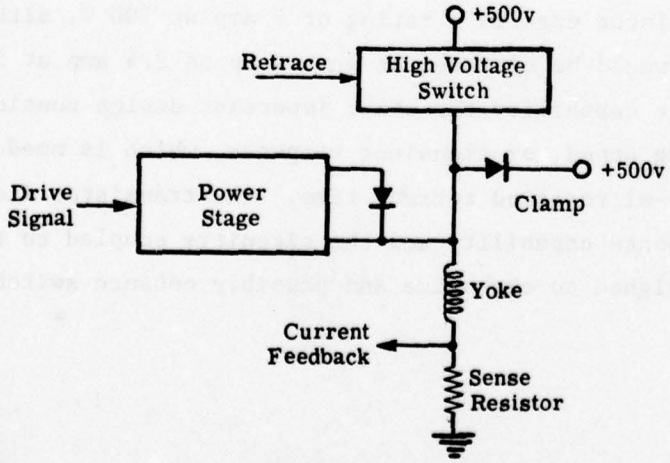

(c) Voltage switchover retrace.

Figure 17. Retrace Circuit Configurations

therefore is used within safe operating parameters. Special consideration is required in the circuit design to assure accurate bias setting of the yoke for centering.

Another approach shown in Figure 17b makes use of an auxiliary inductance which acts as a source of current from a high voltage level for retrace. In this case the normal scan amplifier is single ended. Because the energy transfer capability is not as great, this approach is less attractive than the others considered.

Figure 17c shows the third approach considered which is straightforward in that a high voltage source of the proper polarity is switched across the yoke at the time of retrace. It presents the difficulty of requiring complementary transistors, both of high voltage with one for retrace switching and one for the normal scan amplifier. It may be possible to use a high voltage semiconductor switching device other than a transistor, for example, a gate controlled diode.

All three of these configurations have a potential capability of providing retrace speeds of interest; the development of a design would be required, however, to establish a complete design having the desired performance parameters. We prefer the resonant retrace design of Figure 17a. A high voltage transistor suited to this design is commercially available, for example transistor type 2N6308 (available from Motorola). This transistor carries a rating of 7 amp at 700 V, although for safe operation it would be operated at levels up to 2.4 amp at 500 V. Given this high voltage capability the other important design consideration is high switching speed, or transient response, which is needed to accommodate the sub-microsecond retrace time. The transistor itself must have a rapid response capability and the circuitry coupled to the transistor must be designed to emphasize and possibly enhance switching speed.

SECTION V

EXPERIMENTAL WORK

1. MODIFICATIONS

A number of modifications were made to the present breadboard thermoplastic modulator with the objective of obtaining improved response for 100 MHz bandwith video signals.

One modification was the installation of a special vacuum feed-through for the video signal. It was installed in the envelope neck as close as possible to the electron gun cathode in order to minimize the impedance mismatch to the coaxial feed impedance as discussed in Section III. The effectiveness, i.e., the voltage response across the cathode-to-grid gap of the gun, was not directly measurable. However, using a microscope, the contrast ratio of the grating on the phosphor screen could be judged as a function of input frequency. It was clear that the feed-through improved the overall performance of the system; a frequency of 130 MHz could be observed on the screen.

Observation of the grating on the phosphor screen indicated that system ripple and noise on the deflection circuits was enough to cause the beam to flutter an amount that considerably exceeded 40 μm, which is approximately the grating period for a 100 MHz input signal. Considerable reduction in the flutter was obtained by relocating and shielding circuits and feed cables, replacing leaky capacitors in DC power supplies, and replacing some power supplies with others having less ripple. With these techniques the flutter was diminished to about the 40 μm range. The main effect of the remaining flutter, because of its low frequency nature, was to produce a low frequency wavy effect from scan-line to scan-line (i.e., along the slow scan direction, x) while not affecting the quality of the grating along individual scan lines (i.e., along the fast scan direction, y). Thus, the overall quality of the gratings formed on the thermoplastic was diminished by this effect. It is felt that the flutter could be reduced much further with renewed effort at reducing various noise and ripple sources within the electronics.

An important modification was the redesign of the cathode support structure. This redesign became necessary when the manufacturer (Litton) of our original gun and cathode discontinued supply of replacement parts, including cathodes. Since no direct substitution cathodes were made by other manufacturers, a new cathode support structure was designed to hold a Semi-Con dispenser cathode that could fit into our Litton gun (see Figure 18). Part of the philosophy in designing the new support structure was aimed toward simplifying and speeding up the installation of new cathodes in the gun. The new structure incorporated ceramic disks that were fabricated locally at The University of Michigan's Electron Physics Laboratory. These disks, as well as supporting the cathode, insulated it from the grid and provided the proper grid-to-cathode spacing. Since most of the structure could be assembled, aligned, and spot welded in a special jig external to the gun a new cathode could be mounted in the gun and completely connected in one-half hour after breaking the cathode shipping vial. This installation time was a considerable improvement over that of our previous design, and significantly reduces the potential for cathode contamination during installation.

The operating power for this new cathode was determined by measuring the cathode surface temperature with an optical pyrometer aligned with the throat of the gun, i.e., looking down through the grid and anode apertures and a clear glass faceplate. The proper operating temperature of 1100°C was obtained with about 10 watts of filament power.

We also found it necessary to readjust the grid-to-first-anode spacing because of shorts occurring between them. Part of the glass support rods for the anode were melted and reformed for a new spacing of about 0.004 inch.

2. SYSTEM SWEEP PARAMETER MEASURMENTS

The parameters described in this section were used for all the experiments described in the following section. The spot size (full width at 50% intensity) was measured on the phosphor screen to be

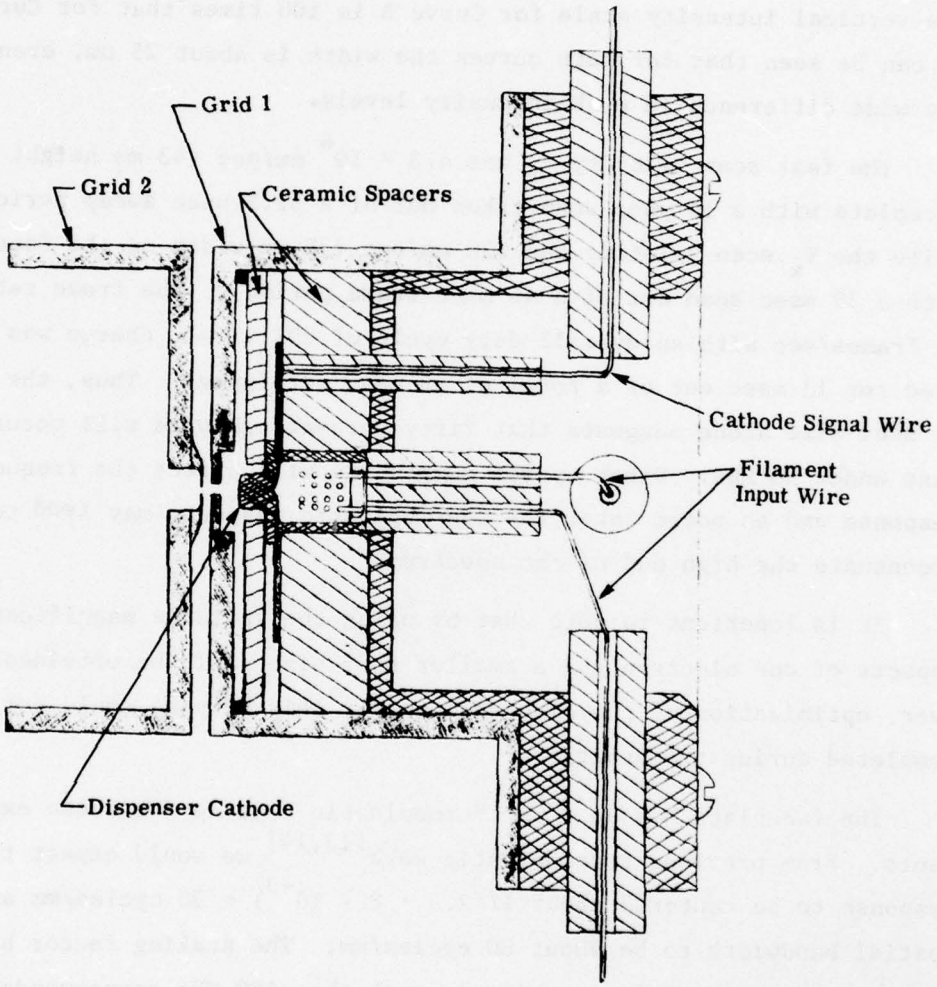

Figure 18. Cathode Support Structure

about 25 μm. Figure 19 shows two photometer scans through the spot for different intensity levels. Curve A was at a low intensity level while Curve B is for a much higher intensity level (about 200 times brighter): the vertical intensity scale for Curve B is 100 times that for Curve A. It can be seen that for both curves the width is about 25 μm, even with the wide difference in peak intensity levels.

The fast scan velocity V_y was 4.3×10^6 mm/sec (43 mm height on faceplate with a 10 μsec scan taken out of a 32.5 μsec sweep period) while the V_x scan velocity was 920 mm/sec (36 mm width on the faceplate with a 39 msec scan out of a 46 msec frame period). The frame rate was 21 frames/sec with an overall duty cycle of 29% (i.e., charge was deposited for 13 msec out of a total of 46 msec per frame). Thus, the effect of spot size alone suggests that fifty percent response will occur at just under 90 MHz. Other system components will affect the frequency response and as noted later the thermoplastic response may tend to accentuate the high end of the spectrum.

It is important to note that by using the variable magnification aspects of our electron gun a smaller spot size could be obtained; however, optimization of the electron gun for this purpose could not be completed during the program.

The faceplate has an 8 μm thermoplastic coating for these experiments. From previous thermoplastic work[13,14] we would expect the peak response to be centered about $1/(2.5 \cdot 8 \cdot 10^{-3}) = 50$ cycles/mm and the spatial bandwidth to be about 80 cycles/mm. The scaling factor between spatial and temporal frequencies is such that 100 MHz corresponds to 23 cycles/mm. Thus, the thermoplastic should respond better to the higher input frequencies.

---

13. Colburn, W.S. and Chang, B.J., "Photoconductor-Thermoplastic Image Transducers," Optical Engineering, pp. 334-343, Vol. 17, No. 4, July-August 1978.

14. Lo. D.S., Johnson, L.H., and Honebrink, R.W., "Spatial Frequency Response of Thermoplastic Films," Applied Optics, 14, 820, April 1975.

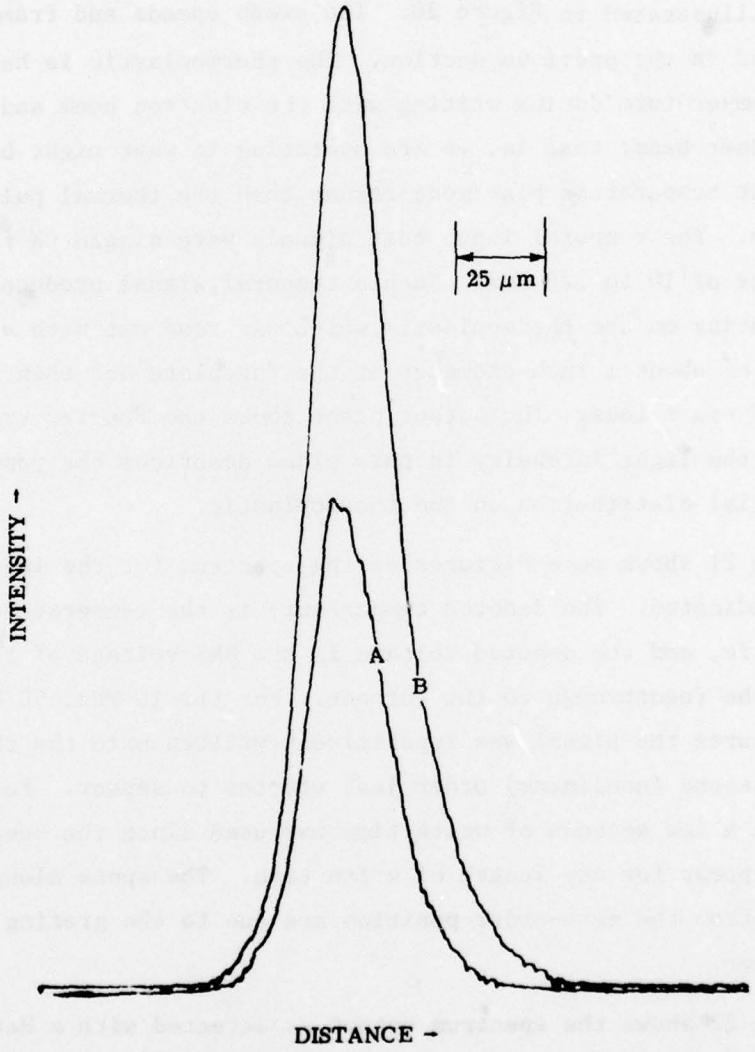

Figure 19. Intensity Distribution of the Writing Beam Spot as Measured on the Phosphor Faceplate

3. THERMOPLASTIC MODULATOR OUTPUT RESULTS

Results described in this section were made with the system schematically illustrated in Figure 20. The sweep speeds and frame rate were as described in the previous section. The thermoplastic is held at a constant temperature during writing with the electron beam and read out with the laser beam; that is, we are operating in what might be called the constant temperature bias mode rather than the thermal pulsed exposure mode. The temporal input test signals were single CW frequencies in the range of 10 to 130 MHz. Such a temporal signal produced a spatial surface grating on the thermoplastic, which was read out with a 6328 Å laser beam of about 1 inch diameter at the faceplate and then Fourier transformed via a lens. The output plane shows the Fourier transform, or rather, the light intensity in this plane describes the power spectrum of the spatial distribution on the thermoplastic.

Figure 21 shows some pictures of the spectrum for the input frequencies indicated. The denoted temperature is the temperature of the thermoplastic, and the denoted voltage is the RMS voltage of the input signal at the feedthrough to the cathode. For the 10 MHz, 50 MHz, and 80 MHz pictures the signal was repetitively written onto the thermoplastic until the second (nonlinear) order just started to appear. For the 110 MHz picture a few seconds of write time was used since the second order would not appear for any length of write time. The spots along the horizontal from the zero-order position are due to the grating formed by the raster.

Figure 22 shows the spectrum output as detected with a Reticon linear array that consists of 1024 silicon photodiodes each of 25 μm by 25 μm size and on a center-to-center spacing of 25 μm. The photodiodes were electronically scanned and the results displayed on an oscilloscope. The detector frame rate was about 10 frames per second. Each picture

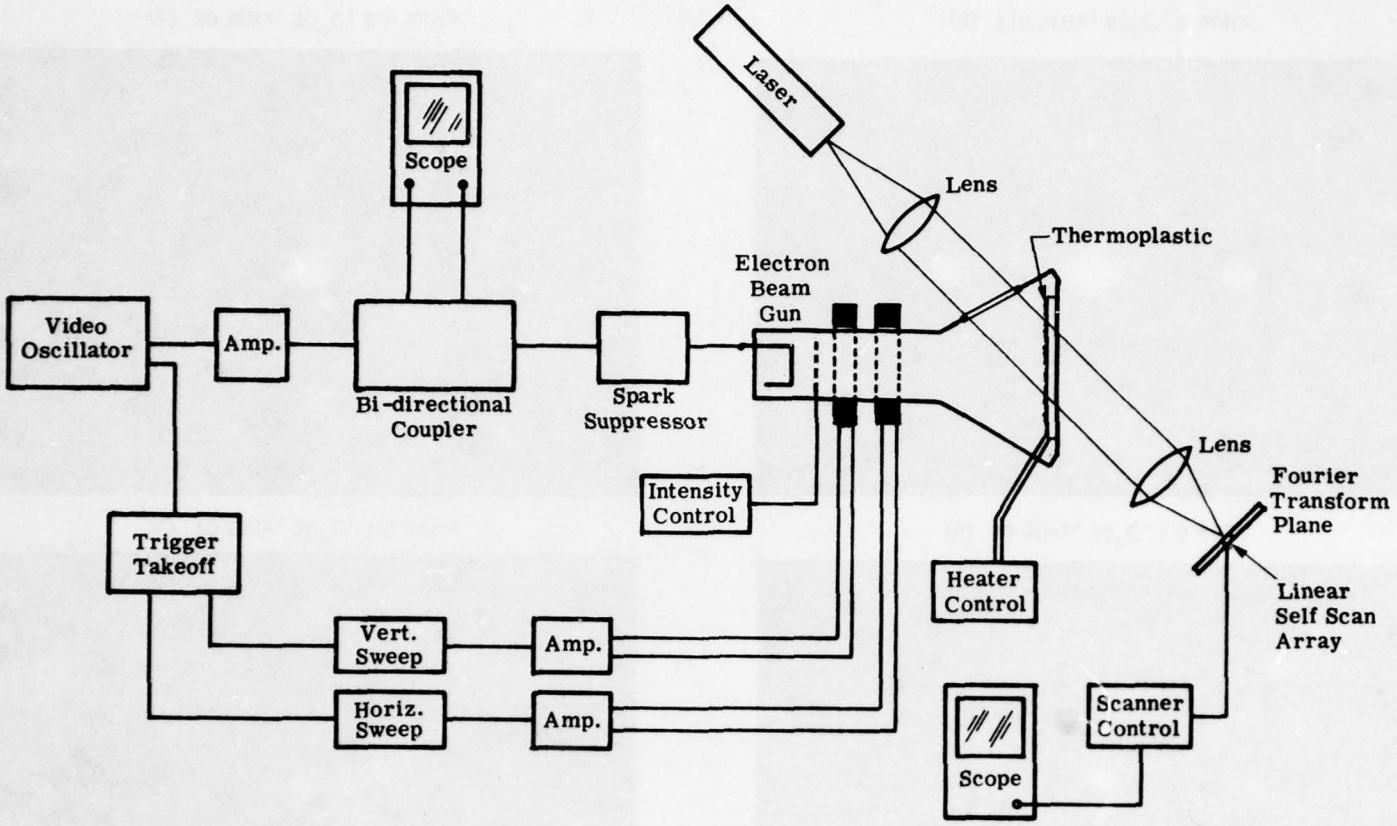

Figure 20. Experimental Setup

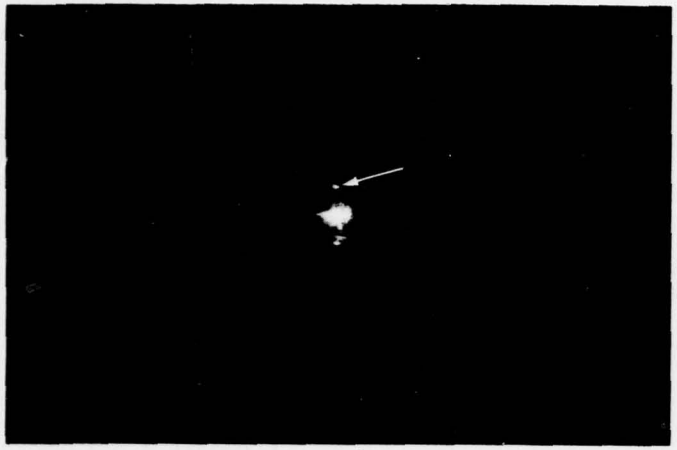

(a) 10 MHz, 50°C, 1.5 volts

(b) 50 MHz, 50°C, 1.5 volts

(c) 80 MHz, 80°C, 2.6 volts

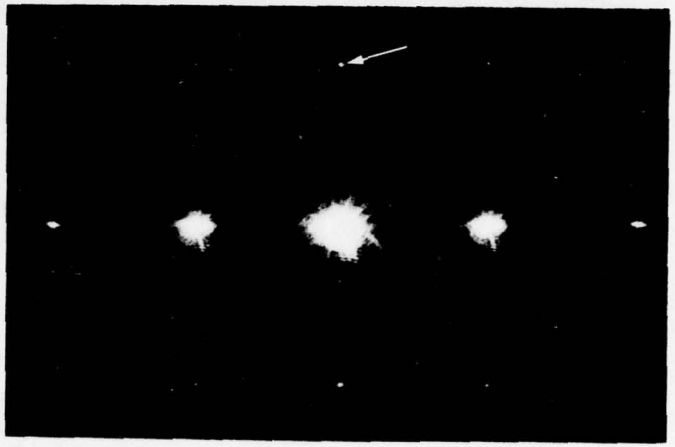

(d) 110 MHz, 50°C, 3 volts

Figure 21. Output Distribution in the Fourier Transform Plane for Single Frequency Inputs

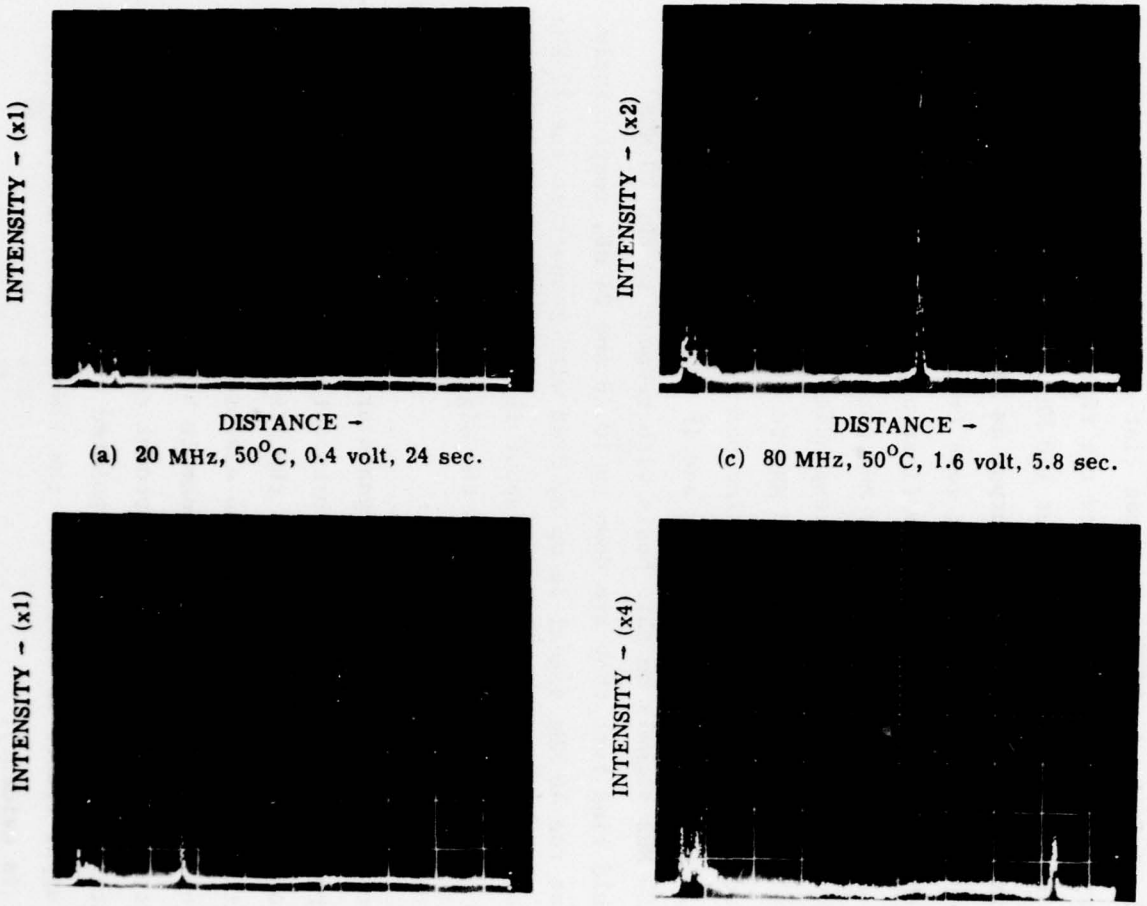

(a) 20 MHz, 50°C, 0.4 volt, 24 sec.

(c) 80 MHz, 50°C, 1.6 volt, 5.8 sec.

(b) 40 MHz, 50°C, 0.5 volt, 2.4 sec.

(d) 120 MHz, 50°C, 1.1 volt, 30 sec.

Figure 22. Reticon Scanned Output of the Distribution in the Fourier Transform Plane

in Figure 22 shows the oscilloscope display for a single detector array scan where the left hand edge of the scan (1st diode) corresponds to zero frequency in the spectrum plane and the right hand edge of the scan (1024th diode) corresponds to about 140 MHz. The orientation of the linear array with respect to the output as shown in Figure 21 is a vertical line extending from the center zero frequency spot in the spectrum upward through the position of the first order diffracted spots. Note that the section from zero to the 7 MHz position has been blocked in order to avoid saturating those corresponding diodes. We could easily detect input frequencies from 10 MHz to over 130 MHz. The signal strength based on a per unit of write time per unit of input signal voltage obviously decreases with frequency and if we were to compare the 80 MHz and 120 MHz signals on this basis with respect to the 20 MHz signal we would find that they are down by 10 dB and 24 dB, respectively. Note also that the 40 MHz signal is up by 2 dB with respect to the 20 MHz signal. Before making any conclusions about the significance of these results, let us consider the buildup of the signal strength as a function of time and spatial frequency.

The time buildup of some output signals are shown in Figure 23. Here, the output spectral component was monitored with a photomultiplier and an oscilloscope. The lower trace shows the status of the unblank signal: where it is at a higher voltage the electron beam is writing at 21 frames/sec, otherwise the input write beam is blanked. The upper trace shows the intensity of the spectral component corresponding to the denoted input frequency. It should be pointed out that full scale intensity in the upper traces is well within the linear region (i.e., no second order is evident).

First notice the lag in signal buildup after the write beam is turned on; it takes time for the thermoplastic to start responding, as would be expected for moving a mass from rest. At the lower temperatures

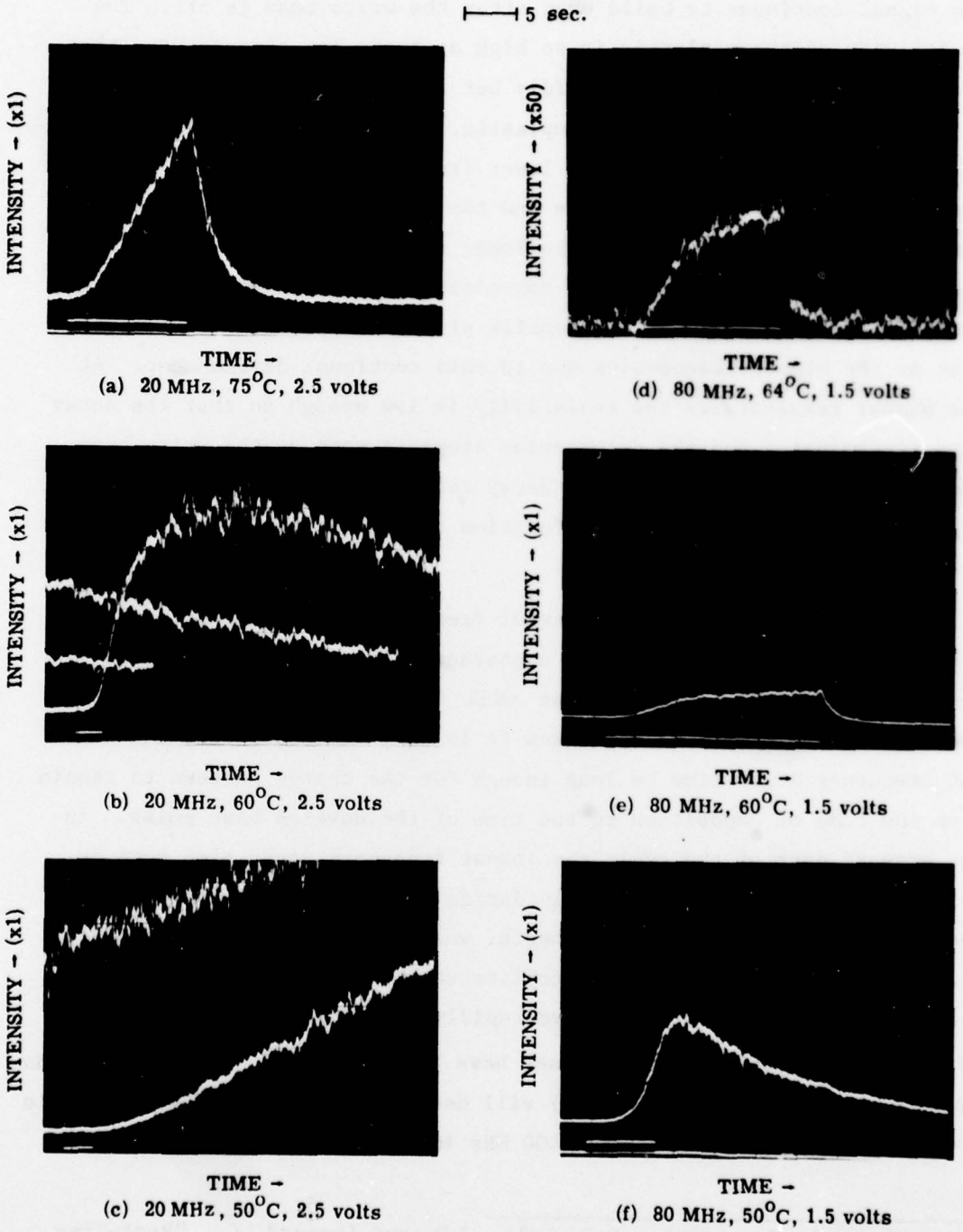

Figure 23. Output Signal Temporal Characteristics

the signal continues to build even after the write beam is off. The resistivity of thermoplastic is so high at these low temperatures that the charges do not dissipate rapidly but rather remain on the surface and continue to deform the thermoplastic. The higher spatial frequencies deform and decay faster than the lower frequencies, apparently since the distance for the mass to move and the charges to diffuse is less for the higher frequencies. Thus, the lower spatial frequencies have a "residual gain" in that the same deposition of peak-to-peak surface charge signal at the lower frequencies produces a greater signal output than at the higher frequencies due to this continual development. At the higher temperatures the resistivity is low enough so that the decay rate predominates and the deformation stops as soon as the write beam stops. Figure 24 shows measured decay rates (i.e., the time for the signal to diminish by 50%) as a function of temperature with spatial frequency as a parameter.

The fact that the higher spatial frequencies respond faster than the lower spatial frequencies is a characteristic of the continuous temperature mode of operation that will limit its applications. In the thermal pulse mode of operation it is only necessary that the highest frequency decay time be long enough for the charge pattern to remain from the time of deposition to the time of the develop heat pulse. In the erasure part of the cycle the lowest frequency decay time must be short enough to decay sufficiently during and immediately following the erase heat pulse. No experimental work in the pulse mode of operation was attempted since the faceplate was not designed for pulse operation (similar faceplates have rapidly deteriorated in past experiments where high energy heat pulses have been applied[15]). The electron write beam current (about 0.1 μA) will need to be increased before single shot operation is possible with 100 MHz input frequencies. Since the

15. Cindrich, I., Currie, G.D., Hall, W.D., and Leonard, C., "Real-Time Modulator for Coherent Optical Processing," ERIM Rept. No. 192300-2-F, Final Rept. on AF Contract No. 33615-72-C-1232, May 1973.

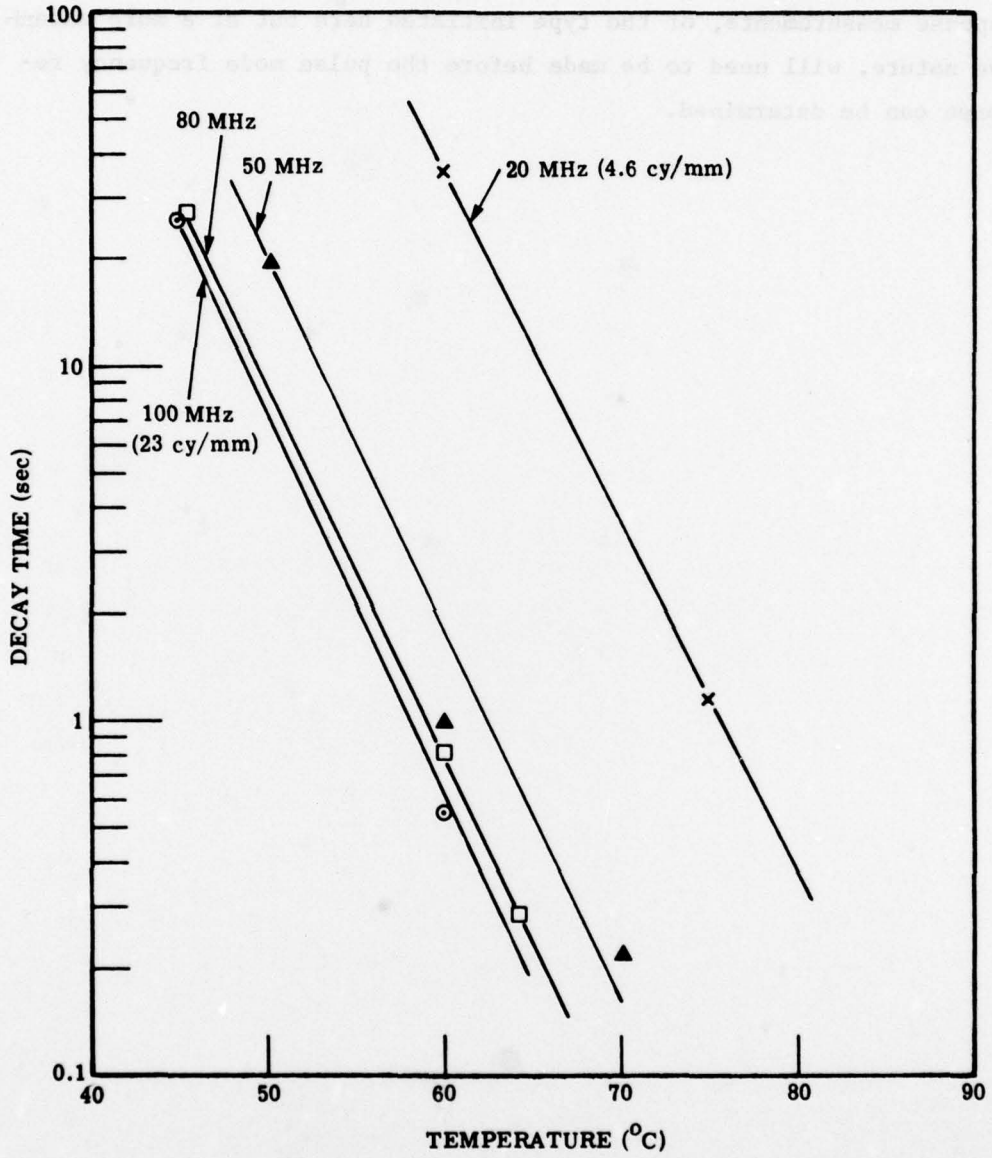

Figure 24. Output Signal Decay Times as a Function of Thermoplastic Temperature

frequency response measured in the continuous temperature mode of operation is not appropriate to the pulse mode of operation, a set of time response measurements, of the type initiated here but of a more extensive nature, will need to be made before the pulse mode frequency response can be determined.

SECTION VI
CONCLUSIONS AND RECOMMENDATIONS

We have described the results of an analytical and experimental research effort to investigate the application of the thermoplastic modulator to wideband spectrum analysis. The objectives of the analytical studies included identification of an approach for increasing the cycling rate of the modulator to 10 frames per second and techniques to extend the modulation bandwidth to 100 MHz. The objective of the experimental investigations was to measure the performance of the breadboard thermoplastic modulator at temporal frequencies of up to 100 MHz.

We achieved the objectives of the analytical studies. Using a computer model to investigate the thermal behavior of the thermoplastic faceplate, we developed a design approach for a faceplate that appears capable of cycling rates of 10 frames per second and that should have minimal effect on the thermoplastic lifetime. The design is based upon a sapphire substrate that is liquid cooled on the rear surface. The high thermal conductivity of the sapphire and the high cooling rate, in combination, will minimize the average temperature of the thermoplastic. In an analysis of the recording system bandwidth, we discussed the system bandwidth in terms of the electron beam modulation, the electron beam spot size, the recording material response, and the sweep speed. We derived an expression for the bandwidth of the electron beam modulation and established component bandwidth goals that would provide a system bandwidth of 100 MHz. Since the duty cycle of the current electron beam deflection circuits is not compatible with the spectrum analysis application, we identified approaches for modifying the circuits with a goal of increasing the duty cycle to 97%.

In the experimental investigations we were less successful in achieving the research objectives; progress was impeded by an unanticipated but required diversion of effort to adapt the electron gun to a new cathode. As a result we were unable to give sufficient attention to reducing the spot size of the electron beam in order to achieve good

response at input frequencies of 100 MHz. We were able to obtain thermoplastic recordings at input frequencies as high as 120 MHz but the response at 100 MHz was down by more than 15 dB. Although the frequency response was less than desired, we were successful in adapting the electron gun to the new cathode design, and in doing so we made significant improvements to the cathode installation procedure. We also improved the performance of the electronics at high frequencies by careful attention to the electronic components and subsystems. Measurements of the deformation decay rates of the thermoplastic showed that under conditions of constant temperature the decay time of a thermoplastic recording is frequency dependent.

As a result of our investigations, we recommend that continued development of the wideband spectrum analysis application concentrate on modification of the breadboard thermoplastic modulator by installation of a sapphire faceplate for rapid cycling and by improvements to the electron gun to reduce the spot size and increase the beam current. To minimize cost, the sapphire substrate should be no more than two to three inches in diameter; a mounting ring would be used to adapt the substrate to the modulator, which now uses a faceplate with a five-inch diameter. Liquid cooling should be provided, and the thermal behavior of the faceplate investigated and characterized prior to mounting to the modulator. An additional modification will need to be made to the modulator to provide reflective readout.

REFERENCES

1. Dusinberre, G.M., Numerical Analysis of Heat Flow, McGraw-Hill, New York, 1949.

2. McAdams, William H., Heat Transmission, Chapt. 2, McGraw-Hill, New York, 1954.

3. Colburn, W.S. and DuBow, J.B., "Photoplastic Recording Materials," Final Technical Report, AFAL-TR-73-255, August 1973.

4. McAdams, William H., Heat Transmission, p. 5, McGraw-Hill, New York, 1954.

5. Headquarters, U.S. Army Material Command, Engineering Design Handbook, Infrared Military Systems, Part One, p. 3-14, AMC Phamphlet No. 706-127, Washington, D.C. April 1971.

6. West, Robert C., Editor, Handbook of Chemistry and Physics, Forty-Ninth Edition, The Chemical Rubber Company, Cleveland, Ohio, 1968.

7. Fink, Donald G., Editor, Electronic Engineers' Handbook, First Edition, p. 6-72, McGraw-Hill Book Company, New York, 1975.

8. McAdams, William H., Heat Transmission, p. 445, McGraw-Hill, New York, 1954.

9. Heikes, Robert R. and Ures, Roland W., Jr., Thermoelectricity: Science and Engineering, Interscience Publishers, New York, 1961.

10. Egli, Paul H., Editor, Thermoelectricity, John Wiley & Sons, New York, 1960.

11. Heikes, Robert R. and Ures, Roland W., Jr., Thermoelectricity: Science and Engineering, Chapt. 15, Interscience Publishers, New York, 1961.

12. Cindrich, I., Currie, G., and Leonard, C., "A Thermoplastic Input Data Modulator for Real-Time Processing of SAR Data," Proceedings of the Technical Program, Electro-Optical Systems Design Conf.-1975, pp. 301-309, November 1975.

13. Colburn, W.S. and Chang, B.J., "Photoconductor-Thermoplastic Image Transducers," Optical Engineering, pp. 334 - 343, Vol. 17, No. 4, July-August 1978.

14. Lo, D.S., Johnson, L.H., and Honebrink, R.W., "Spatial Frequency Response of Thermoplastic Films," Applied Optics, 14, 820, April 1975.

15. Cindrich, I., Currie, G.D., Hall, W.D., and Leonard, C., "Real-Time Modulator for Coherent Optical Processing," ERIM Rept. No. 192300-2-F, Final Rept. on AF Contract No. 33615-72-C-1232, May 1973.

*U.S.Government Printing Office: 1978 — 657-002/261